Australian Government
Bureau of Meteorology

The Centre for Australian Weather and Climate Research
A partnership between the Bureau of Meteorology and CSIRO

Improvements in atmospheric physical parameterizations for the Australian Community Climate and Earth-System Simulator (ACCESS)

Zhian Sun et al.

CAWCR Technical Report No. 061

www.cawcr.gov.au

Improvements in atmospheric physical parameterizations for the Australian Community Climate and Earth-System Simulator (ACCESS)

Zhian Sun et al.

The Centre for Australian Weather and Climate Research
- a partnership between CSIRO and the Bureau of Meteorology

CAWCR Technical Report No. 061

April 2013

Authors:	Zhian Sun, Charmaine Franklin, Xiaobing Zhou, Yimin Ma, Hongyan Zhu, Vaughan Barras, Greg Roff, Patricia Okely, Lawrie Rikus, Ben Hu, Daohua Bi, Martin Dix, Simon Marsland, Hailin Yan, Nicholas Hanna, Maciej Golebiewski, Arnold Sullivan, Harun Rashid, Petteri Uotila, Tony Hirst, and Kamal Puri
Title:	Improvements in atmospheric physical parameterizations for the Australian Community Climate and Earth-System Simulator (ACCESS)
ISBN:	978-1-922173-64-5 (Electronic Resource)
Series:	CAWCR technical report.
Notes:	Includes bibliographical references and index.
Subjects:	Numerical weather forecasting--Australia.
	Atmosphere--Mathematical models.
	Climatology--Mathematical models.
	Meteorology--Mathematical models.
Dewey Number:	551.630994

Contact details

Enquiries should be addressed to:

Zhian Sun

Centre for Australian Weather and Climate Research:

A partnership between the Bureau of Meteorology and CSIRO

GPO Box 1289, Melbourne

Victoria 3001, Australia

z.sun@bom.gov.au

Copyright and Disclaimer

Contents

List of figures

List of Tables

1. INTRODUCTION

The Australian Community Climate and Earth-System Simulator (ACCESS) is a new coupled ocean and atmosphere climate modelling system being developed at the Centre for Australian Weather and Climate Research (CAWCR). ACCESS uses the UK Met Office Unified Model (Met UM, Davies et al. 2005) as its atmospheric component, which is coupled with the GFDL Ocean Model version 4.1 (MOM4p1, Griffies et al. 2009) and the Los Alamos National Laboratory Sea Ice Model version 4.1 (CICE4, Hunke and Lipscomb 2010), using the numerical coupler OASIS3.25 (Valcke 2006). The development of ACCESS has followed the implementation of the numerical weather prediction (NWP) system developed by the UK Met Office which uses the Met UM for atmospheric prediction with a 4-DVAR assimilation system.

One of the primary purposes for the development of the ACCESS system is to provide the Australian climate community with a new generation fully coupled Earth atmosphere modeling system for climate research and applications. The (uncoupled) system is also used in the Bureau of Meteorology for operational NWP forecasting, where it has demonstrated significant improvement in forecast skill compared to previous systems (Puri et al. 2010). The initial implementation of the ACCESS system started in 2007 and has been officially operational at the Bureau since the 17 August 2010. It has also been used to perform the experiments for analysis studies, supporting the Fifth Assessment report of the Intergovernmental Panel on Climate Change (IPCC AR5) and the Coupled Model Intercomparison Project phase 5 (CMIP5) (Taylor *et al.* 2012).

A special issue on ACCESS model development and evaluation is currently under preparation and will be available soon in the Australian Meteorological and Oceanographic Journal. This report is to document modifications and improvements to the ACCESS atmospheric model. Due to the reasons described by Bi *et al.* (2013a), two versions of the model were chosen for the IPCC AR5 experiments and they are distinguished by their atmospheric and land surface components; the ocean and sea ice components are the same in both. The first model version is referred to as "ACCESS1.0" which uses the Met UM model configured for the HadGEM2 atmospheric physics and the Met Office's MOSES land surface model (Martin *et al.* 2011). The second model version is referred to as "ACCESS1.3" which includes significant new atmospheric physics, similar to that of the Met Office GA1.0 (Hewitt *et al.* 2011). A major difference between HadGEM2 and GA1.0 is the cloud scheme. HadGEM2 uses the modified diagnostic cloud scheme of Smith (1990) while GA1.0 uses a new prognostic cloud scheme PC2 (prognostic cloud prognostic condensate; Wilson *et al.* 2008a). Importantly, ACCESS1.3 includes the "Community Atmosphere Biosphere Land Exchange" land surface scheme (CABLE, Kowalczyk *et al*. 2006).

The successful implementation of the Met UM in the ACCESS system has involved significant technical and scientific efforts, especially with the ACCESS1.3 version. This is because the initial Met UM GA1.0 model was configured for use with a different ocean model (NEMO, Madec, 2008) and because it was a step towards the development of HadGEM3, which has continued with subsequent GA releases (e.g. Walters *et al.* 2011). Thus considerable tuning and adjustments experiments were required to make the overall model performance satisfactory. For this reason, a series of test runs were performed to evaluate model performance and several modifications to the Met UM atmospheric physics, MOM4p1 ocean model and sea ice model were made to correct problems identified from the test runs. Since the most modifications were conducted for establishing ACCESS1.3, the results presented in this report are only from this version of the model. The modifications to the ocean and sea ice models have been described in separate papers. This report will present modifications to the Met UM atmospheric physics. It should be noted that although CABLE has been included in this version, it was not available during the course of conducting this series of test experiments. Therefore, all results presented in this report do not include CABLE.

Some modification and development work was conducted using the ACCESS single column model (SCM) and AMIP type climate experiments. This is because they run much faster than the full coupled-model so the modifications can be quickly evaluated. The results from SCM runs can also be compared directly with observations. Results from some of these experiments are also included in this report.

Finally, physics development work outside of that intended for immediate use in CMIP5 or operational NWP is also described here. This longer-term research, for example in the area of PBL parameterisation and the use of superparameterization methods for convection, is intended to impact the design of future systems, or to provide underpinning support for parameterisation development.

2. MODIFICATIONS OF ATMOSPHERIC MODEL PHYSICS FOR IMPROVING SST SIMULATION IN ACCESS1.3

The first version of the ACCESS coupled model with the Met Office UM configured for the prototype HadGEM3 atmospheric physics had a significant cold sea surface temperature (SST) bias. Although cold SST bias is a common problem in most coupled systems (Lin, 2007; Luo et al. 2005; Jungclaus et al. 2006), the biases in ACCESS were larger than those documented errors from other models. Figure 1 shows the distribution of the SST difference between the averaged SST from 100 years of the ACCESS model integration and the observed global climatological SST data (http://www.nodc.noaa.gov/OC5/WOA05/pr_woa05.html). It is evident that cold SST biases exist in almost the entire northern hemisphere, with larger biases along the tropical equatorial region where the maximum cold SST error is about -6 K. In contrast, warm SST biases occur in the southern ocean between 30 oS and 70 oS. Although the cold SST bias in the North Atlantic Ocean is larger than the biases in the tropical region, the performance in the tropics is a major concern in coupled-models because this is a key area linked to climatic variability such as the El Niño-Southern Oscillation (ENSO). The ACCESS-OM benchmarking experiment (Bi et al. 2013b) using CORE normal year forcing (Large and Yeager (2004)) does not show such a large cold bias, suggesting that the cold biases in ACCESS model may result from the MetUM atmosphere. In order to confirm this and find solutions to improve the simulations, a large number of testing experiments have been conducted. These tests cover the radiation, clouds, convection and surface wind stress. These works will be described in the following sub-sections.

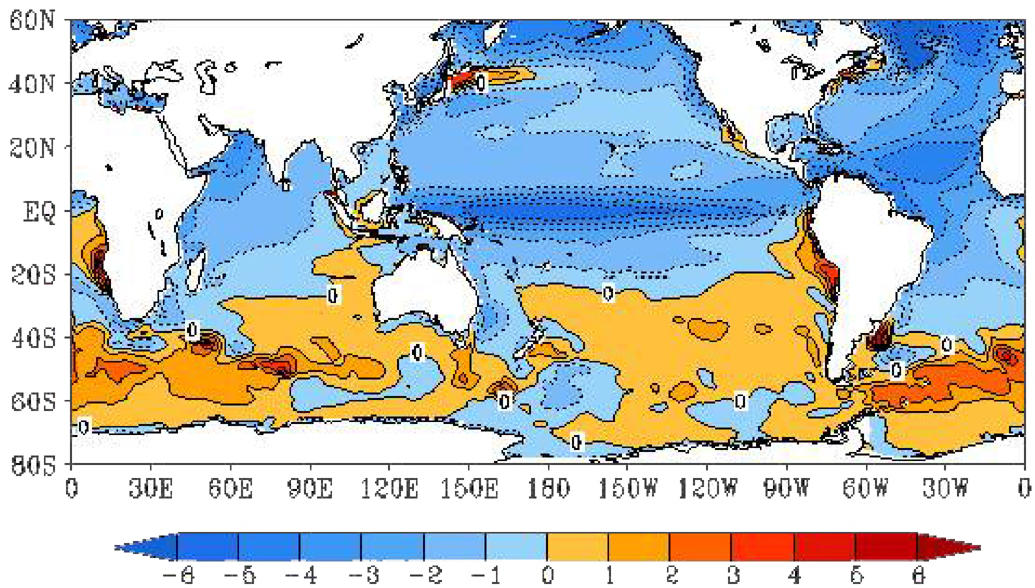

Fig. 1 SST difference (K) between the averaged SST from 100 years of the ACCESS model integration and the observed global climatological SST data.

2.1 Possible reasons for the cold SST bias

Solar radiation can penetrate the ocean, heating the sea water down to about 500 meters, depending on the water clarity. Sensitivity studies have shown that the solar radiation absorbed in the upper few metres significantly influences intraseasonal SST variations through changes in the amplitude of diurnal SST variation (Shinoda, 2005). A second factor that influences the SST is the atmospheric surface wind stress that largely determines the distribution of the oceanic surface current (OSC) and subsequently the distribution of the SST. Luo et al. (2005) tested different levels of OSC coupling in a CGCM and concluded that a full inclusion of OSC in the physics of the atmospheric surface layer was required to reduce the Tropical Pacific SST bias.

Chen *et al.* (1994) investigated the roles of vertical mixing depth, solar radiation, and wind stress in an ocean model simulation of the SST in the tropical Pacific Ocean using a hierarchy of numerical experiments with various combinations of vertical mixing algorithms and surface-forcing data. They found that the SST seasonal cycle can be well simulated by improving the representation of the vertical mixing layer depth, but the accurate annual mean SST cannot be confidently reproduced without more accurate forcing data. Chen et al. (1994) used three different products of solar radiation as forcing to run an ocean model and the difference between these data is, on average, 40-60 W m^{-2}. The SST simulated using these solar radiation data can differ by as much as 6K. They also tested three different wind stress forcing data sets and found that SST can be 2K cooler when the wind stress is stronger. From these experiments they concluded that any attempt to attribute the annual mean SST errors to model deficiencies would not be successful until the uncertainty in the surface heat flux is greatly reduced.

In order to understand the reasons behind the SST biases in ACCESS, we first analysed the surface energy budget and compared the results with observations. We use the surface latent and sensible heat flux dataset from the project of the Objectively Analyzed air-sea Fluxes (OAFlux) for the Global Oceans (Yu and Weller, 2007) and the surface shortwave (SW) and longwave (LW) radiation data from the International Satellite Cloud Climatology Project (called ISCCP-FD) (Zhang *et al.* 2004) as the benchmark to evaluate ACCESS model results. The OAFlux and ISCCP-FD data are available at 3-hour time steps from 1983-2009. These data are averaged into a long term annual mean climatology.

Figure 2 shows a comparison of each heat flux component at the ocean surface and the difference between the modelled values and observations. Panel A shows the net downward SW flux. It is seen that the bias in net downward SW flux is negative in the Northern Atlantic Ocean and tropical equatorial Ocean, and positive in the southern hemisphere with larger biases in the belt between 45°S – 70°S. The excess net solar radiation in the Southern Ocean is a common problem in most climate models (Wild 2005; Trenberth and Fasullo, 2010; Haynes *et al*. 2011) and Bodas-Salcedo *et al.* (2008, 2012) have investigated this issue within the context of the Unified Model. Our focus here is on the ACCESS configuration and specifically on the negative bias in net solar radiation from the west coast of South America towards the Tropical Warm Pool in the Tropical equatorial Ocean, which is roughly the area where the cold SST biases occur, although the area of SST bias extends further west. There is also positive bias in SW going from Central America westwards into the tropical Pacific. The negative bias in the tropical equatorial region attracts our attention as it is possible that the cold SST bias may be due to insufficient solar energy entering into the ocean.

The net LW flux differences in Fig.2b show a positive bias in the latitude belt around 45 ^{o}S. Since the positive LW bias means lost energy from the ocean surface it can partially cancel the positive net SW bias in this region. The LW biases in the tropics and northern hemisphere are relatively small, indicating that the LW bias may not be responsible for the cold SST bias in these regions.

We now move to look at the turbulent heat fluxes. Figure 2c shows the observed latent heat flux（OAFlux） and the difference between the modelled and observed values. It can be seen that the model produces positive biases over the large tropical and Southern Ocean areas. These positive biases imply that the ocean is losing heat to the atmosphere and may lead to a cooling of the SST. The actual relationship between SST and latent heat flux, however, is more complicated and cannot be explained by thermodynamic considerations alone. It usually involves the interaction between convection and the large-scale circulation (Zhang and Mcphaden, 1995). The sensible heat fluxes are displayed in Fig.3d and they show that the magnitude of this component is much smaller than the latent flux, and the difference between the model and OAFlux is also small except in the high latitude Southern Ocean, the China Sea and Northern Atlantic Ocean. There is a positive bias in the Southern Ocean corresponding to the warm SST bias there and a negative bias in the China Sea and Northern Atlantic Ocean.

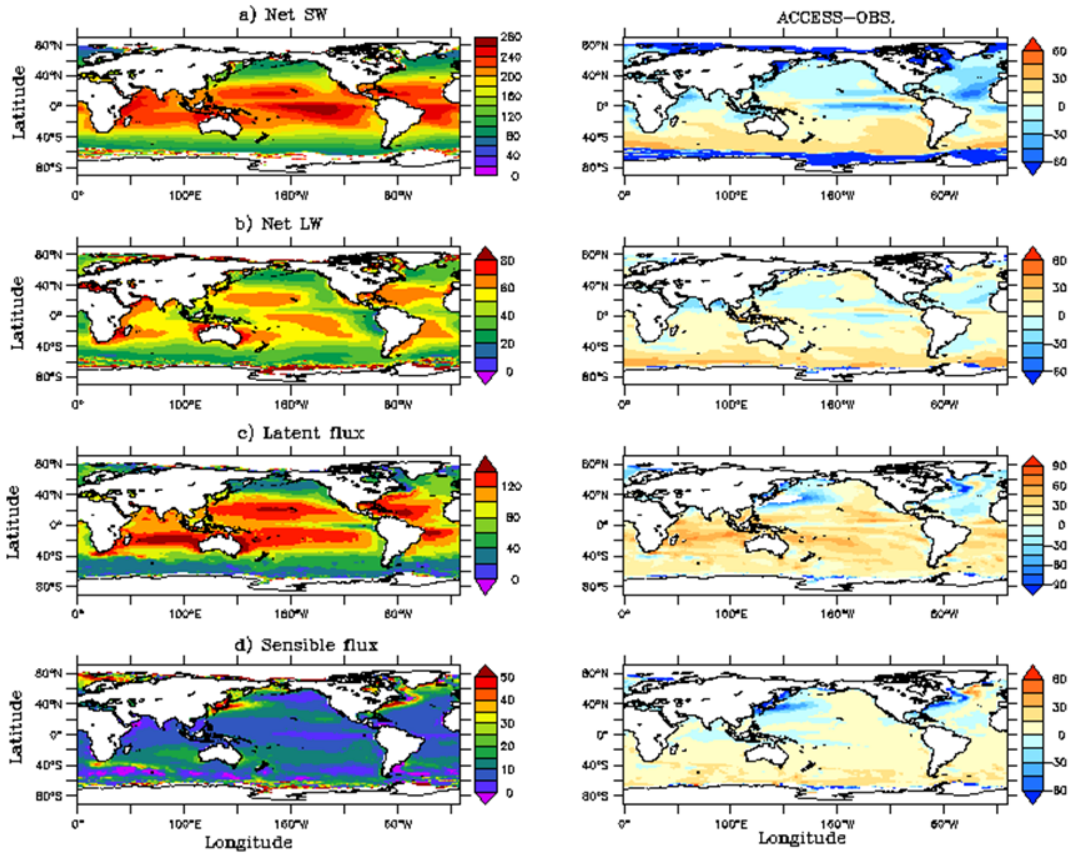

Fig. 2 Comparison of the surface heat flux components (a: net downward SW, b: net upward LW, c: latent heat, d: sensible heat) from OAFlux and ISCCP-FD (left column) and the differences between ACCESS and these references (right column).

We also checked the wind stress generated by ACCESS and compared the result with that from the second version of the climatological forcing dataset Coordinated Ocean-ice Reference Experiments (COREv2, Large and Yeager, 2008). Fig. 3 shows biases in the zonal surface wind stress (ACCESS minus COREv2). The areas with positive biases represent weak zonal wind stress there. It is seen that the wind stresses over the tropical Pacific Ocean, Southern Ocean, Northern Pacific and Northern Atlantic are all underestimated by the ACCESS model. As discussed by Chen *et al.* (1994), the weaker wind stress usually results in warmer SST, especially over the Eastern Pacific Ocean because both upwelling cold water and advective heat flux will be weak. Therefore, the cold SST bias in the tropical Pacific Ocean is unlikely due to the effect of wind stress. However, the positive wind stress biases over the Southern Ocean could contribute to the warm SST biases there.

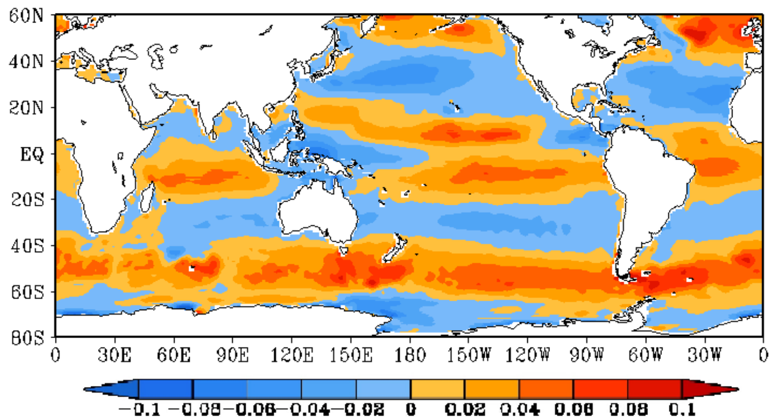

Fig. 3 Bias in annual mean zonal wind stress (ACCESS minus COREv2)

We now focus our attention on the surface heat flux. The above energy budget analysis indicates that larger biases exist in both the SW radiation and the latent heat fluxes and these errors could be the reasons behind the cold SST biases in the tropical equatorial regions. Although the interaction between latent heat flux and SST is complicated due to the involvement of convection and large-scale circulations as mentioned earlier, the reduction of solar radiation at the tropical ocean surface certainly causes a cooling effect. Since the solar radiation at the surface is greatly affected by clouds, our first effort to minimize the SST errors in the model was focused on improving the representation of cloud in the UM. This includes improving: the prediction of cloud-fraction; the horizontal distribution of cloud water/ice content in a grid-box as seen by the radiation scheme and the vertical overlap assumptions for multiple cloud layers. In addition to the modifications to UM clouds, we also modified the air-sea flux scheme that leads to an improvement in the simulation of surface wind stress.

The methods used to conduct these modifications have been described in relevant papers (Shonk *et al.* 2010; Franklin *et al.* 2012; Ma *et al.* 2012; Boutle and Morcrette, 2010). Only brief summaries are given below.

2.2 Representation of the effect of horizontal structure of cloud on radiation

Clouds are very complex in structure and interact strongly with radiation. Hence they are a very important aspect of the climate system and need suitable representation in climate models. However, the representation of cloud in climate models is relatively simple due to model resolution and computational limitations. Two main approximations are commonly used in most modern general circulation models when representing clouds in the radiation scheme. The first is the plane-parallel approximation in which the horizontal structure of a cloud is represented by a single homogeneous region of cloud in a grid box layer. Using this approximation the effect of cloud on radiation in each grid box layer can be determined by just two quantities: a cloud fraction and a single value of cloud water/ice content. While this treatment is computationally efficient, such a simple cloud structure usually overestimates the radiative effects of cloud (Barker and Davies, 1992; Carlin, *et al.* 2002). The second approximation concerns the cloud vertical structure. Cloud is aligned vertically according to an overlap assumption. Most GCMs use the maximum-random overlap assumption (Geleyn and Hollingsworth, 1979), namely that two cloud layers are maximally overlapped if they are vertically continuous and randomly overlapped if they are separated by a clear layer.

Shonk *et al.* (2010) developed a cloud horizontal inhomogeneity parameterization based on radar observations. They named this parameterisation the "triple-cloud" scheme, where they divide a homogeneous cloud layer into two separate columns: an optically thin layer and an optically thick layer. The cloud water/ice content for the sub-columns is assigned values via the equation:

$$W_{sub} = \overline{W} \pm f_W \overline{W} \quad , \qquad (1)$$

where $\overline{W}$ is mean cloud water/ice content provided by the model's cloud scheme for a gridbox; f_W = 0.75 is the fractional standard deviation of cloud water/ice content and was determined by radar observations. The radiative transfer calculations through the cloud are then performed twice: once for the thin layer and once for the thick layer. By doing so the effect of sub-grid scale inhomogeneity of cloud in a gridbox is taken into account. This representation can be easily implemented in the ACCESS model because the Edwards and Slingo radiation scheme (Edwards and Slingo, 1996) used in ACCESS has a function to split a grid box layer into columns of clear, convective and stratiform clouds, thus giving three regions in the layer and maintaining the vertical coherence of convective cloud. The scheme also has a solver to deal with the radiative transfer calculations for three columns simultaneously in the layer so that the extra computational time is minimized. This triple cloud scheme has been implemented into the ACCESS model. The splitting of cloud water/ice by Eq. (1) is assigned to the stratiform and convective clouds in the layer, respectively, and this leads to a significant improvement in the simulation of SST (see results in the following section).

2.3 Vertical exponential-random overlapping parameterization

The vertical overlap assumption influences the cloud amount used in radiation calculations. Sensitivity studies have shown that small changes in global cloud amount result in noticeable biases in the global radiation budget (Randall *et al.* 1984; Slingo, 1990). Such changes in global cloud amount can easily be introduced due to uncertainty in the cloud parameterization and inaccurate representation of the vertical cloud overlap. Barker *et al.* (1999) and Wu and Liang (2005) used data from a cloud-resolving model (CRM) and calculated the radiative fluxes through clouds using a radiative transfer code. They found biases in the TOA short-wave flux caused by using the random overlap assumption in place of the exact overlap that were non-negligible in size with respect to plane-parallel biases.

Hogan and Illingworth (2000) used radar data from Chilbolton to derive cloud overlap statistics and establish ‘true’ total cloud cover from two adjacent cloud layers. They then calculated cloud cover for pairs of cloud layers using maximum, random and maximum-random overlap and compared the values with the ‘true’ cloud cover from the radar data. They found that for pairs of cloud layers separated by at least one layer of clear sky, the clouds were overlapped randomly. However, for pairs of layers in vertically continuous cloud, the overlap varied with the vertical separation of the layers from maximum to random. They introduced an ‘overlap parameter’, α, as a measure of the degree of correlation between cloud positions in a pair of layers,

$$\beta = \alpha\beta_{max} + (1-\alpha)\beta_{rand} \quad (2)$$

where β represents actual overlap, the subscript *max* and *rand* represent maximum and random overlap, respectively. $\alpha = 1$ implies maximum overlap, and $\alpha = 0$ implies random overlap. Hogan and Illingworth (2000) also calculated the variation of overlap parameter α with layer vertical separation. For discontinuous cloud, they found the overlap parameter to be approximately zero for all separations, indicating random overlap in this case. For continuous cloud, they found a near-exponential decrease of the overlap parameter with vertical separation distance Δz. They derived the following expression to describe the variation of overlap parameter with vertical separation Δz:

$$\alpha = \exp\left(-\frac{\Delta z}{Z_{0\alpha}}\right), \quad (3)$$

where $Z_{0\alpha}$ is a decorrelation height and related to the vertical resolution and the horizontal domain size. By analyzing radar data at different locations, they found that $Z_{0\alpha}$ varies with latitude ϕ and can be expressed by

$$Z_{0\alpha} = 2.899 - 0.0275\phi \quad . \quad (4)$$

This approach, in which cloud overlap is a function of vertical separation of two layers and latitude is referred to as the "exponential-random overlapping" scheme.

2.4 Modification to the PC2 ice cloud-fraction

There are two cloud schemes available in the ACCESS atmospheric model. The diagnostic scheme of Smith (1990) with modifications (Wilson *et al.* 2004) and a new prognostic cloud scheme "PC2" (Wilson and Bushell, 2007; Wilson *et al.* 2008a). The ice condensate is a prognostic variable in both schemes. The cloud fraction from the Met UM when using the diagnostic scheme is the sum of the cloud fraction from the largescale cloud scheme of Smith (1990) and a diagnostic convective cloud fraction described by Gregory (1999). The PC2 scheme includes prognostic variables for the cloud liquid-water content, the cloud ice-water content, the bulk cloud fraction, the liquid cloud fraction and the ice cloud fraction.

Franklin *et al.* (2012) have evaluated these two schemes using the Met UM single column model (SCM) together with field observations from the Tropical Warm Pool–International Cloud Experiment (TWP–ICE). They found that the ice cloud fraction from the PC2 scheme was underestimated due to an assumption that ice depositional growth increases the cloud ice water content but not the cloud ice fraction. This assumption greatly reduces the correlation between ice water content and ice cloud fraction compared to that observed. Franklin *et al.* (2012a) modified the ice cloud fraction formulation of PC2 by including the effect of depositional growth on the ice cloud fraction,

$$\Delta C_i = A\left(1 + \frac{\Delta \overline{qi}}{\overline{qi}(A/C_i)}\right)^{1/2} - A\,, \qquad (5)$$

where C_i is the ice cloud fraction, A is the area of the grid box that contains ice and is above ice saturation, $\overline{qi}$ is the grid box mean ice water and $\overline{qi}(A/C_i)$ is the amount of ice that is present in the region of the grid box where deposition is occurring, and $\Delta\overline{qi}$ is the source of IWC from depositional growth. This expression allows the ice cloud fraction to vary as a function of the vapour depositional growth rate of ice and gives more realistic variations in the PC2 cloud fractions as shown in Fig. 9 of Franklin *et al.* (2012). It will be shown in the following section that this modification leads to improved simulations of the cloud amount, cloud radiative forcing and SST in the ACCESS coupled-model.

2.5 Modification to thePC2 water cloud fraction

Cloud fraction is the area of a model grid-box covered by cloud. Although it represents a percentage area covered by clouds, it is assumed that all clouds fill the grid box in the vertical direction to ensure a consistent treatment of solar and thermal-infrared, clear-air and cloudy radiative fluxes at the top and bottom of each model layer. Observations (human observer, ground-based facilities and satellites) provide cloud fraction in the horizontal extension, or 'area cloud fraction' while the PC2 scheme, like most other GCMs, parameterizes cloud fraction as the volume of cloud in a grid box. Fig. 4 demonstrates the difference between the area fraction C_a and the volume fraction C_v, from which we can see that C_a is always equal to or greater than C_v and the difference changes with the vertical dimension of the grid box. Wilson *et al.* (2007) proposed a novel solution to improve the determination of the area cloud fraction in the Smith diagnostic cloud scheme. In this method, the thermodynamic profiles are interpolated or extrapolated onto three sublevels within a cloud layer and the diagnostic cloud scheme is run on each of the sublevels. C_a for the cloud layer is assigned as the maximum value of C_v from the three sublevels and this is used within the radiation scheme. Boutle and Morcrette (2010) implemented this method into the PC2 scheme to correct cloud fraction for liquid water cloud due to the effects of coarse vertical resolution. This scheme was implemented in UM7.3 for ACCESS1.3

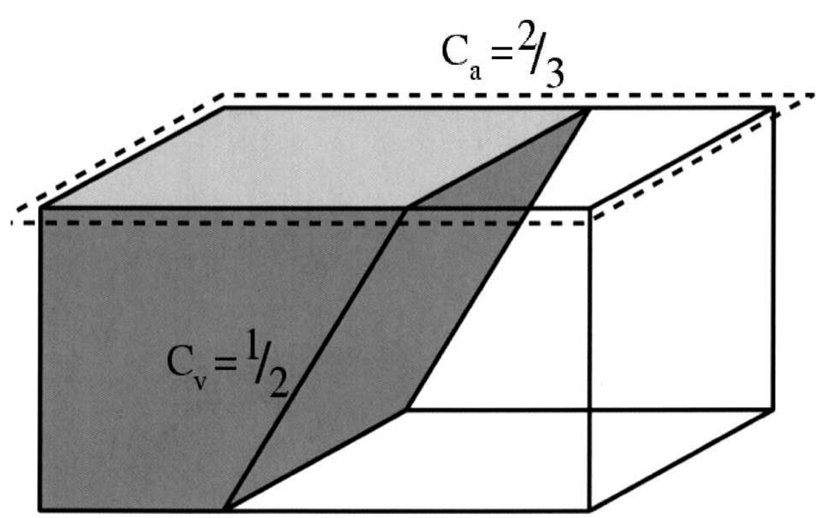

Fig. 4 Schematic of a distribution of clouds within a 3D grid box, where the cloud fraction by volume (C_v) is 1⁄2, but the cloud fraction by area (C_a) is 2⁄3. (after Brooks *et al.* 2004)

2.6 Modifications to the air-sea flux scheme

Air-sea exchanges in a coupled ocean-atmosphere model are important to the accurate simulation of SST because the atmospheric surface stress exerted on the ocean surface is largely responsible for the distribution of the oceanic surface current (OSC) and subsequently the distribution of the sea surface temperature (SST). Based on Monin-Obukhov similarity theory (MOST, e.g. Garrat, 1994, p38), “bulk” algorithms to estimate the air-sea interface fluxes for momentum, sensible and latent heat can be expressed as

$$\frac{\overrightarrow{\tau_0}}{\rho_0} = c_m V(\overrightarrow{u_{z1}} - \overrightarrow{u_{osc}}) \ , \qquad (6)$$

$$\frac{H_0}{C_p \rho_0} = -c_s V[(T_{z1} - T_{z0s}) + \frac{g}{C_p}(z_1 - z_{0m} - z_{0s})] , \qquad (7)$$

$$\frac{E_0}{\rho_0} = -c_s V(q_{z1} - q_{z0s}) , \qquad (8)$$

where *u*, *T*, *q* are wind speed, air temperature and specific humidity, respectively, ρ_0 is the air density near the surface, C_p is the specific heat for air, g is gravitational acceleration. z_1 is referred to as the near surface height within the atmospheric surface layer, and z_{0m} and z_{0s} are momentum and scalar roughness lengths. Surface exchange coefficients for momentum flux (c_m) and scalar (sensible and latent heat) flux (c_s) are found via

$$\sqrt{c_m} = \frac{\kappa}{\ln(z_1 / z_{0m}) + \Psi_m(L, z_1 + z_{0m}, z_{0m})} , \qquad (9)$$

$$c_s = \frac{\kappa}{\ln(z_1 / z_{0s}) + \Psi_s(L, z_1 + z_{0m}, z_{0m})} \sqrt{c_m} , \qquad (10)$$

where κ is the von Kármán constant and L is the Monin-Obukhov length. . Ψ_m and Ψ_s are are empirical functions to allow for stability corrections**.** The momentum and scalar roughness lengths z_{0m} and z_{0s} in the above equations are important parameters that influence the derived surface fluxes in a coupled model. In the Met UM model, they are determined using the Charnock relation for z_{0m}

$$z_{0m} = \frac{0.11\gamma}{b + u_*} + \frac{\alpha}{g} u_*^2 , \qquad (11)$$

and the dependence of z_{0s} on z_{0m} and u^* is given by

$$z_{0s}=\begin{cases}\max[\dfrac{2.52\times10^{-6}}{u_*+b}, & \dfrac{2.56\times10^{-9}}{z_{0m}}] \quad \text{Low winds condition}\\ \max[\dfrac{2.56\times10^{-9}}{z_{0m}}, & 7\times10^{-8}] \quad \text{High winds condition}\end{cases} \tag{12}$$

where γ is kinematic viscosity, b is a small constant to avoid z_{0m} becoming singular at $u_*=0$. α is the Charnock parameter which is normally taken as a constant, e.g. α=0.018 is recommended although there is scope for some variation. Ma et al. (2012) compared the z_{0m} and z_{0s} values derived using the formulae above against results from field programs and found that discrepancies exist. They then constructed a new expression for z_{0m} with a variable Charnock parameter, together with a new scheme for z_{0s}. The Charnock parameter to represent the momentum roughness in Eqn (11) is thus modified as a function of surface wind speed to,

$$\alpha=(\alpha^{\max}-\alpha^{\min})\frac{\tanh[C^{rate}(U_{10n}-U_{10n}{}^{mid})]+1}{2}+\alpha^{\min}, \tag{13}$$

U_{10n} is the 10 metre neutral wind, and the other quantities are fitting coefficients. The scalar roughness length is calculated as

$$z_{0s}=\begin{cases}\max[\dfrac{2.52\times10^{-6}}{u_*+b}, & fz_{0s}(U_{10N})] \quad \text{Low wind condition}\\ \max[fz_{0s}(U_{10N}), & 1.12\times10^{-5}] \quad \text{High wind condition}\end{cases}, \tag{14}$$

$$\ln[fz_{0s}(U_{10n})]=(\ln z_{0s}{}^{i}-\ln z_{0s}{}^{i-1})\frac{U_{10n}-U_{10n}{}^{i-1}}{U_{10n}{}^{i}-U_{10n}{}^{i-1}}+\ln z_{os}{}^{i-1}, \quad i=2,3,\dots,n. \tag{15}$$

where z_{0s}^{i} is special scale roughness length at special knots of U_{10n}^{i}.

Figure 5 shows a comparison of the results for the new expression for α against those from field experiments, a constant value used in the standard UM7.3 model and the formulation used in COARE3.0 (Fairall *et al.* 2003).

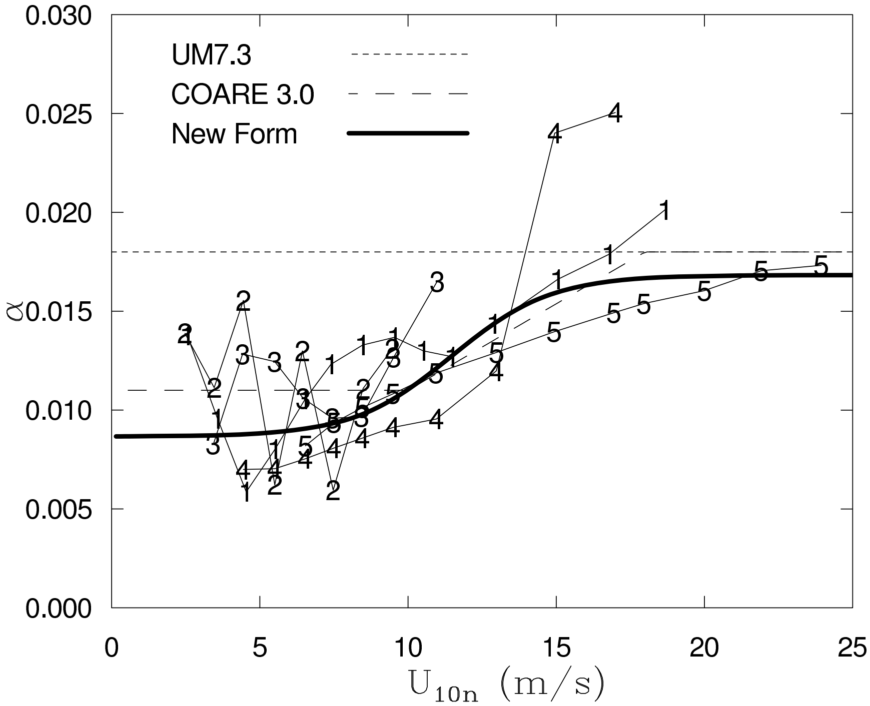

Fig. 5 Estimates of Charnock parameters from various field experiments and evaluations: 1, Fairall *et al* (2003) evaluation; 2, COARE; 3, SCOPE; 4, MBL; 5, Yelland and Taylor (1996). The values from the standard UM7.3 model, COARE 3.0 and the new formulation are also shown

It is evident that the constant value used in the Met UM is higher than most of the experimental data. The results from the new formulation well represent the field experiment data and are close to those from COARE 3.0. The evaluation of the modified scheme in the ACCESS model is given in the following section.

3. EVALUATION OF PHYSICAL MODIFICATIONS IN ACCESS1.3

In this section, the atmospheric physical modifications described above are tested in ACCESS1.3. The integration of the ACCESS model was performed for 120 simulated years for each experiment using present-day conditions. The results for the last 100 years are averaged to generate the model climatology that is then compared with corresponding values from satellite observational climatology. Cloud amounts from CALIPSO (Cloud-Aerosol Lidar and Infrared Pathfinder Satellite Observation) and cloud radiative forcing at the top of the atmosphere from ISCCP-FD (International Satellite Cloud Climatology Project) are compared against the model products. We use results from five test cases to illustrate the impacts of these physical parameterisation modifications on the equilibrium states of ACCESS1.3. 100 years of integration may not be long enough for the model to establish true equilibrium but it is adequate for testing purposes. The first case is a control run (CNTL) without any change to the model physics. This run produces a large

SST cold bias as shown previously in Fig. 1. Four experiments were then performed subsequently to test the impact of our modifications. The first experimental run (EXP1) includes the effects of the inhomogeneous cloud distribution scheme triple cloud. The second (EXP2) is the same as EXP1 but adding the modification of ice cloud fraction. The third (EXP3) is the same as EXP2 but including the modification to the surface roughness length. The fourth (EXP4) is the same as EXP3 but using the exponential-random overlap scheme. The area cloud correction scheme has been applied to all four experiments but the results are not analysed separately because its effect on SST is less significant than the others.

3.1 Cloud field

We first examine the cloud fields as they are a critical component of the radiation budget and the Earth's climate. Although the ISCCP cloud data are normally used to evaluate model clouds, they are not used in this work since the ISCCP clouds at Polar Regions are not reliable due to the effect of high surface reflectance (Rossow *et al.* 1993). The ISCCP algorithm also has a limitation in being unable to detect thin cirrus clouds, which may result in an underestimation of high level cloud amount (Chevallier *et al.* 2004). We use CALIPSO cloud amounts instead because the instruments of CALIPSO have finer vertical resolution, are sensitive to thin cirrus clouds and can detect clouds right down to the surface. Five years of data from 2006 to 2010 are available and these observations represent the climatological characteristics of clouds. The results presented in this and next subsection do not include those of EXP3 because the modification to the surface stress has little effect on the cloud and radiation fields.

Figure 6 shows the five year mean total cloud fraction determined using the CALIPSO data (a) and the differences between ACCESS modelled values and CALIPSO values (b-f). Figure 6b presents the total cloud amount error from the results of the control run relative to CALIPSO. It is seen that the total cloud amounts are generally underestimated over the whole globe except in the equatorial Pacific Ocean and Northern Atlantic Ocean. The underestimate of cloud cover by the PC2 scheme was documented in Franklin *et al.* (2012). Even after the implementation of the area correction scheme this problem still exists. Implementation of the inhomogeneous cloud scheme in the radiation calculations does not help to improve the cloud amount simulation. Instead, it results in a further reduction of cloud amount as seen in Fig. 6c. Although the reduction of total cloud amount in the eastern central equatorial region facilitates a correction to the cold SST bias, the cloud radiative effects in other areas are poorly simulated as seen in the next section. Implementation of the modified ice cloud fraction parameterization improves the model total cloud amount significantly as seen in Fig. 6d. The underestimate of cloud cover in EXP1 that occurred over the whole globe is reduced. The negative biases in the Polar Regions are changed to positive biases, indicating the correction scheme has a large effect in cold regimes. Modifying the vertical cloud overlap changes the total column cloud cover. Figure 6f shows that replacing maximum-random cloud overlap method with exponential-random overlap scheme causes noticeable changes in total cloud amount. The values in the northern polar region and the southern ocean are increased and those over the southern polar region and the tropics are decreased (these changes can only be seen by difference between EXP4 and EXP2which are not shown here).

We further compare cloud amount at different heights. Figure 7 shows the results for high cloud amounts. The high cloud amounts from the control run are underestimated from middle to low latitudes and overestimated in the southern high latitude ocean and the north polar region. The model high cloud amounts are not large enough in the deep convection areas such as the tropical warm pool, central Africa and South America. Since high clouds over the tropics have a warm effect, insufficient high level cloud amount in these areas may be partially responsible for the cold SST bias seen in Fig. 1. Implementation of the inhomogeneous cloud scheme causes further reductions in high cloud cover as seen in Fig. 7c. The systematic underestimation of high cloud cover in the EXP1 is largely corrected by the ice fraction correction scheme as shown in Fig. 7d. The improvement in the tropical regions is quite significant, leading to a better longwave radiative forcing simulation which will be shown in the next section. However, the high cloud amounts in high latitude regions from this run are larger than the observations. The changes in cloud vertical overlap result in a slight reduction of high cloud cover in the tropics, but cause some modest increases in in high cloud in the high latitudes.

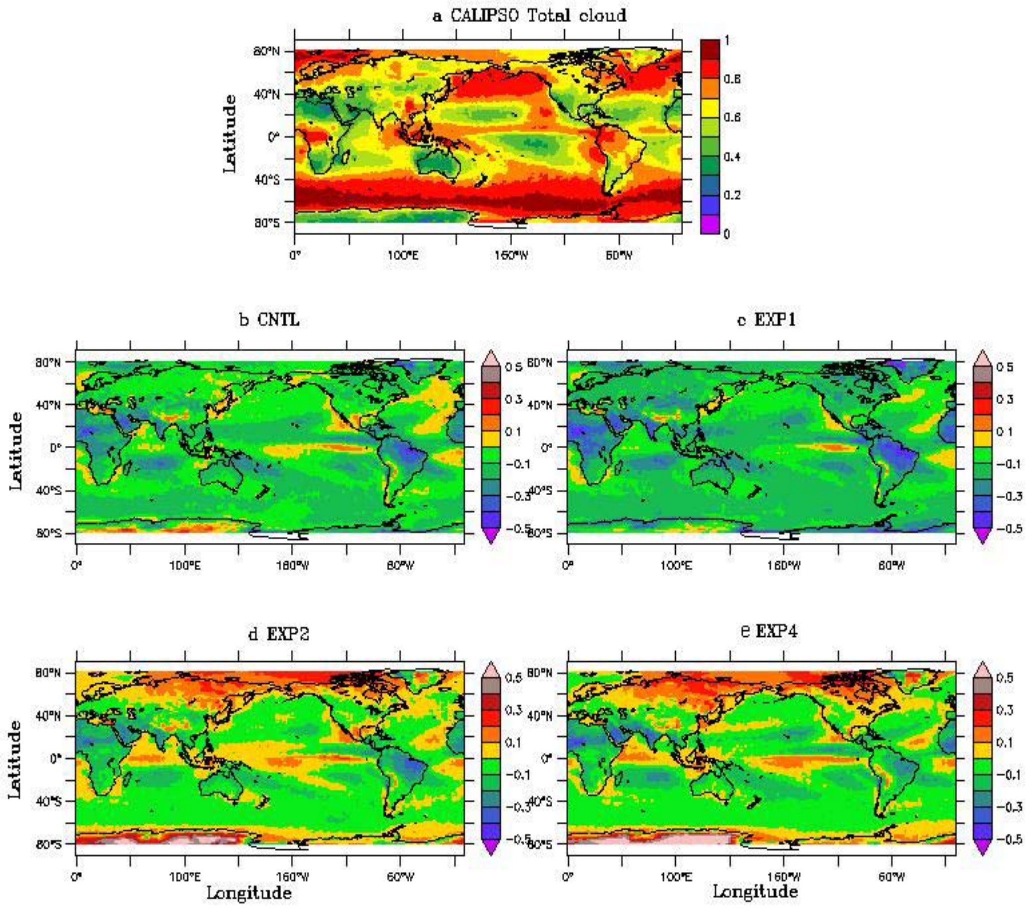

Fig. 6 Comparisons of total cloud amount between CALIPSO measurements and ACCESS modelled values. Panel a shows CALIPSO total cloud fraction. Panels b – f are difference between model and CALIPSO.

The comparison for middle cloud is shown in Fig. 8. The middle level cloud amounts in the control run are underestimated over the tropics but mostly overestimated in the middle-high latitudes. Similar to the high cloud case, the effect of the inhomogeneous cloud scheme is to decrease the middle cloud and it results in the best comparison among the four test runs. Again, the modified ice cloud fraction scheme leads to increases of the middle cloud amount in middle-high latitudes. The change in the vertical overlap scheme leads to a slight increase in middle cloud in the northern polar region. However, it should be noted that CALIPSO midlevel cloud fraction could be underestimated in regions of thick cloud due to attenuation of the lidar

The comparison for low clouds is presented in Fig. 9. The control run generates excess low level clouds in the equatorial pacific, Northern Pacific, Eastern and northern Atlantic Ocean, Tibetan Plateau and Antarctic. The low cloud amount is less in the Indian Ocean, Africa, South-eastern

Pacific and South America. Implementing the inhomogeneous cloud scheme has little effect on low level clouds. The use of the modified ice cloud fraction parameterization results in increases of low cloud in high latitudes. This indicates that there must be a lot of low level ice cloud in these regions. Implementing the vertically exponential-random overlap scheme slightly increases low level clouds in high latitudes.

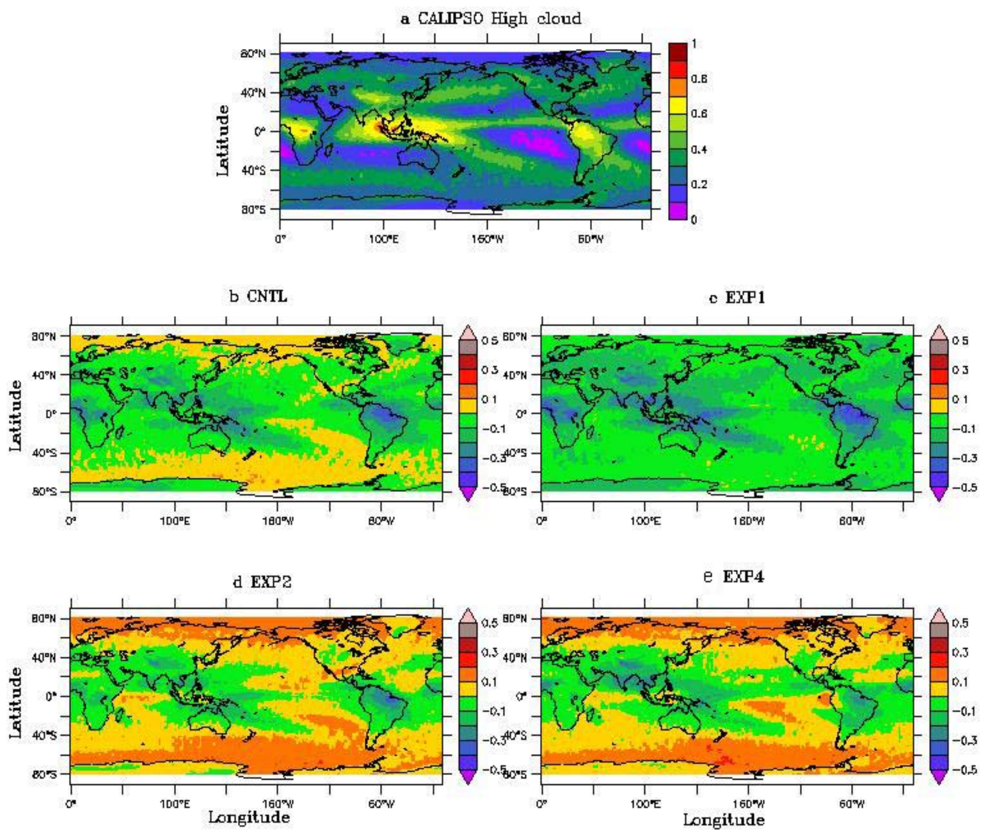

Fig. 7 Same as Fig. 6 but for high cloud amount.

It should be noted that the methods used to determine the cloud amount by CALIPSO are different from that used in the model. This may cause some inconsistency. Franklin *et al.* (2012) evaluated ACCESS model clouds from AMIP experiments using the COSP (the Cloud Feedback Model Intercomparison Project (CFMIP) Observational Simulator Package). In that study the model cloud amounts are determined in the same way as for CALIPSO, so that the results are more consistent than those in this paper. The results from Franklin *et al.* have shown that the middle level cloud fraction is underestimated in ACCESS AMIP experiments which is consistent with the result from the similar experiment performed by Bodas-Salcedo *et al.* (2012) using MetUM GA1.2. The inconsistent result for middle level cloud found in this work is likely due to the cloud-analysis method used in the current coupled-model.

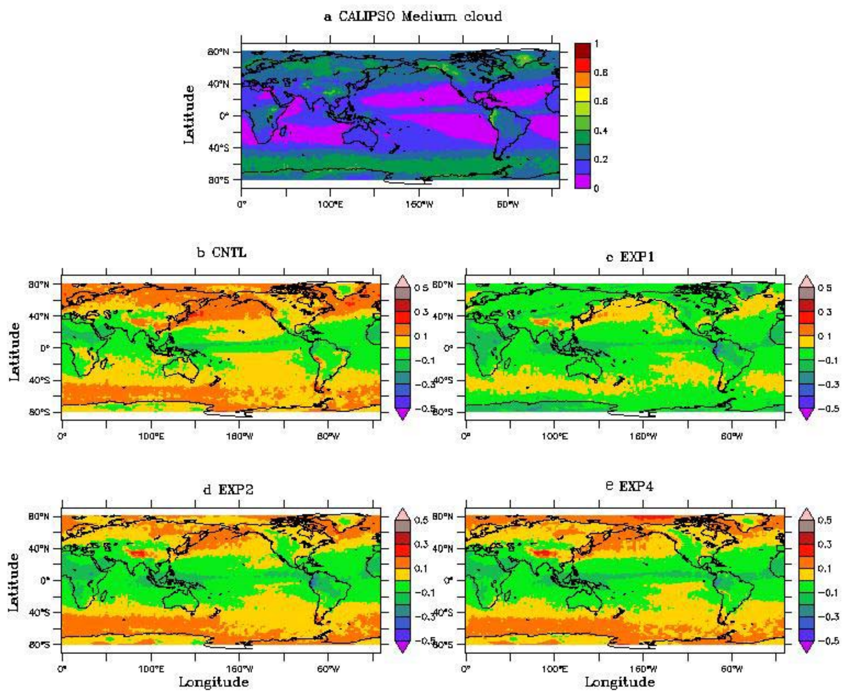

Fig. 8 Same as Fig. 6 but for middle clouds.

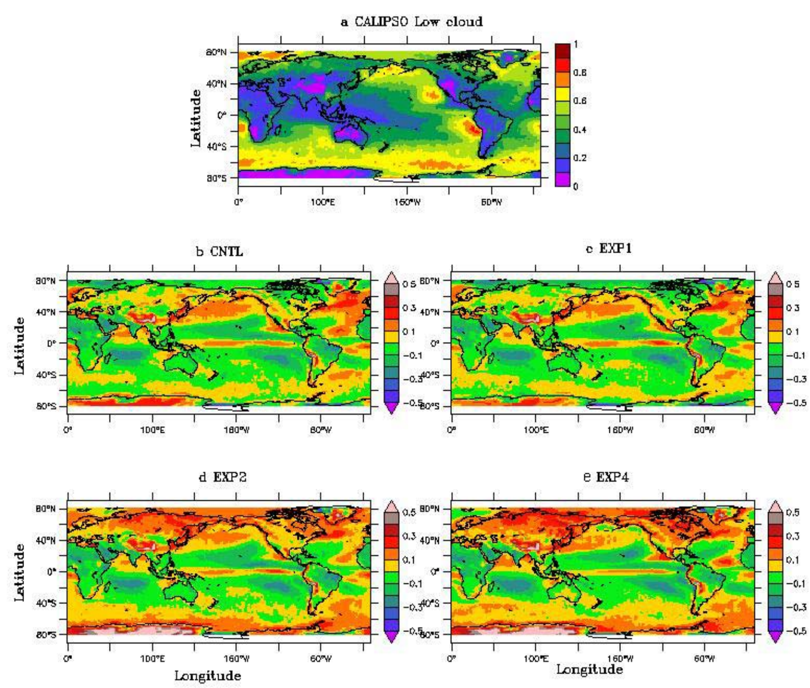

Fig. 9 Same as Fig. 6 but for low clouds.

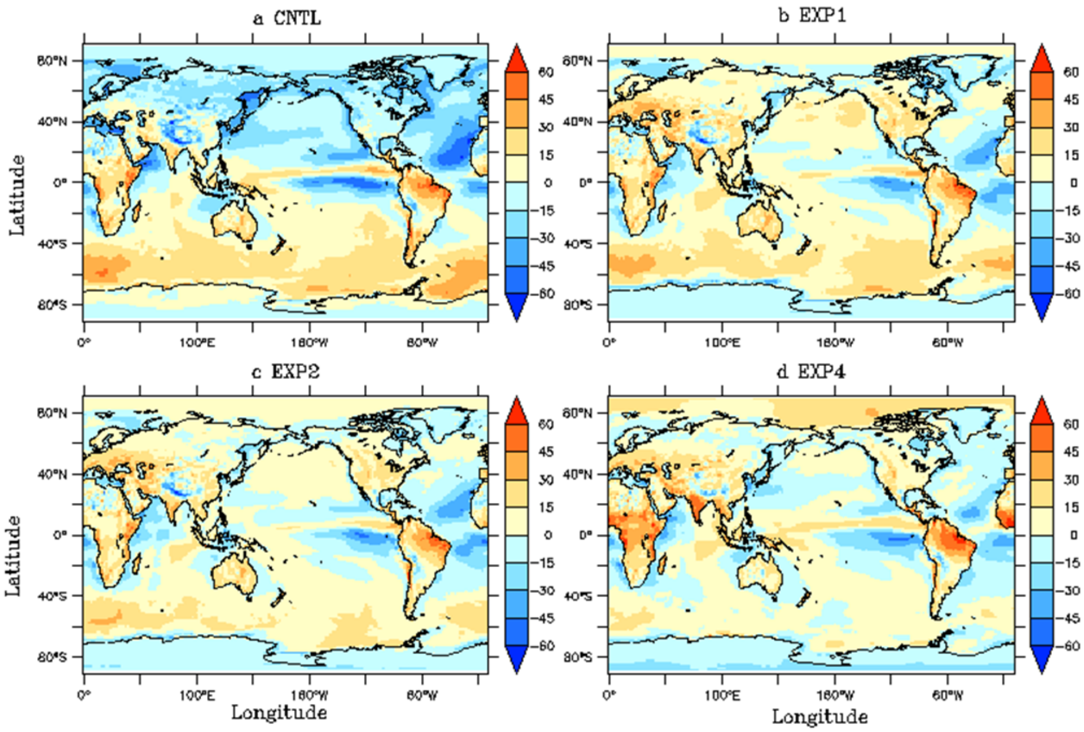

Fig. 10 Biases in net downward solar radiation at surface (ACCESS model minus ISCCP-FD).

3.2 Radiation fields

The solar radiation absorbed by the ocean surface layer is an important factor that has a direct influence on the SST. To be useful, any modification to the model physics must result in improvements to the net solar radiation at the surface in order to improve the SST simulation. Figure 10 shows a comparison of biases in the net downward solar radiation at the surface before and after the modifications described in the earlier section. As has been mentioned earlier, the original Met UM used a plane-parallel homogeneous cloud approximation in the radiation calculations and this resulted in an overestimation of cloud effects on the surface solar radiation. As seen in Fig. 10a the net solar radiation in the northern hemisphere was generally underestimated while that in the southern hemisphere was overestimated. The underestimation of the downward solar radiation in the northern hemisphere in the ACCESS model is largely due to the effect of the inaccurate representation of cloud inhomogeneity in a grid box. Replacing the homogeneous cloud liquid/ice water content with the triple clouds thin and thick column values in the radiation calculations improves the modelled net solar radiation significantly in the northern hemisphere as seen in Fig. 10b. The negative biases from the east coast to central equatorial Tropical Ocean, east coast of China and Atlantic Ocean are all reduced. It is interesting to see that some positive biases in the southern hemisphere are also reduced. This is due to the correction of water cloud fraction using the area cloud correction scheme.

Inclusion of the modified ice cloud fraction scheme further improves the net solar radiation simulation. It is seen from Fig. 10c that the positive biases shown in Fig. 10b are clearly reduced, especially in the southern ocean but the negative biases in the tropical ocean are not increased. A shift to the exponential-random overlap scheme causes increases in the net solar radiation in the tropical warm pool, tropical land areas, and the North Pole, which increases the error. The warm bias in the southern ocean is further reduced with the inclusion of this overlap scheme.

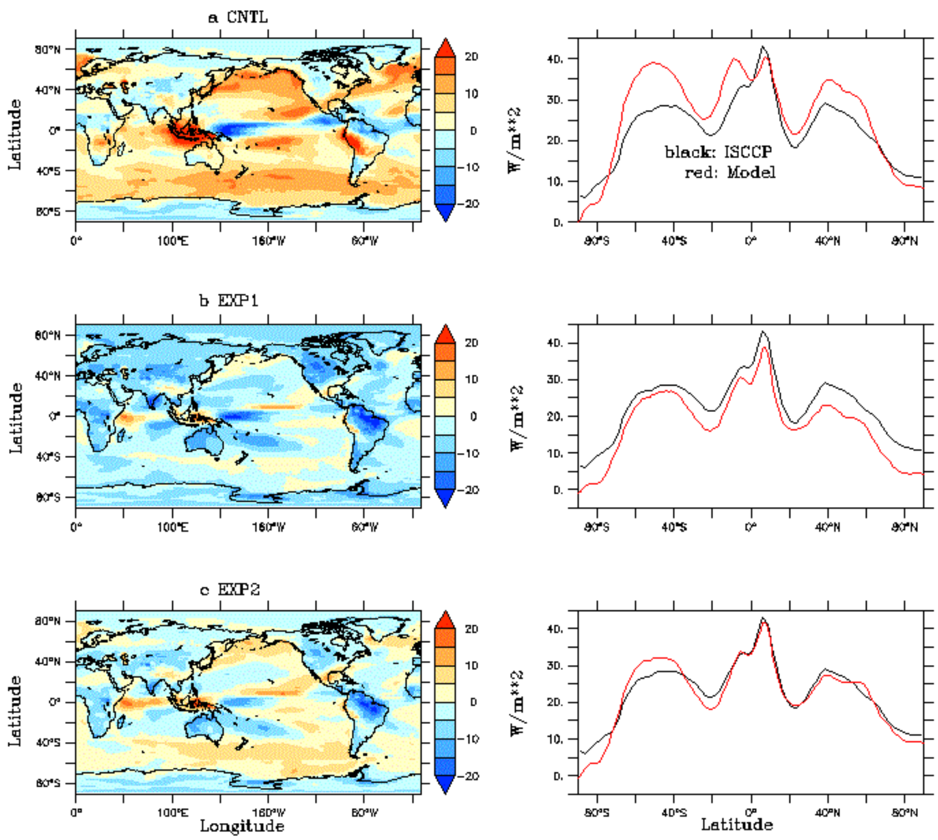

Fig. 11 Biases in cloud longwave radiative forcing (left column) and zonal mean distribution of longwave forcing (right) from three ACCESS model runs. The cloud radiative forcing determined by the ISCCP-FD is used as a benchmark.

Figure 11 shows the results of cloud longwave radiative forcing (LRF) difference between model simulations and observation. The control run results in excess longwave forcing along the middle latitude storm track in the northern hemisphere and most parts of the southern ocean. These excess LRF are clearly due to the excess high level cloud covers as shown in Fig. 8. A shift to the triple cloud inhomogeneous scheme leads to a significant improvement in the longwave radiation in the Southern Hemisphere midlatitudes. The positive biases in the Southern Ocean are reduced dramatically, but results for the Northern hemisphere are less accurate. The negative biases over the northern hemispheric become larger than those from the CNTL run. This is due to the reduction in the middle and high level cloud amounts as seen in Figs 8c-9c. This reduction is corrected by the modified ice cloud fraction scheme and the LRF is further improved as seen in Fig. 11c.

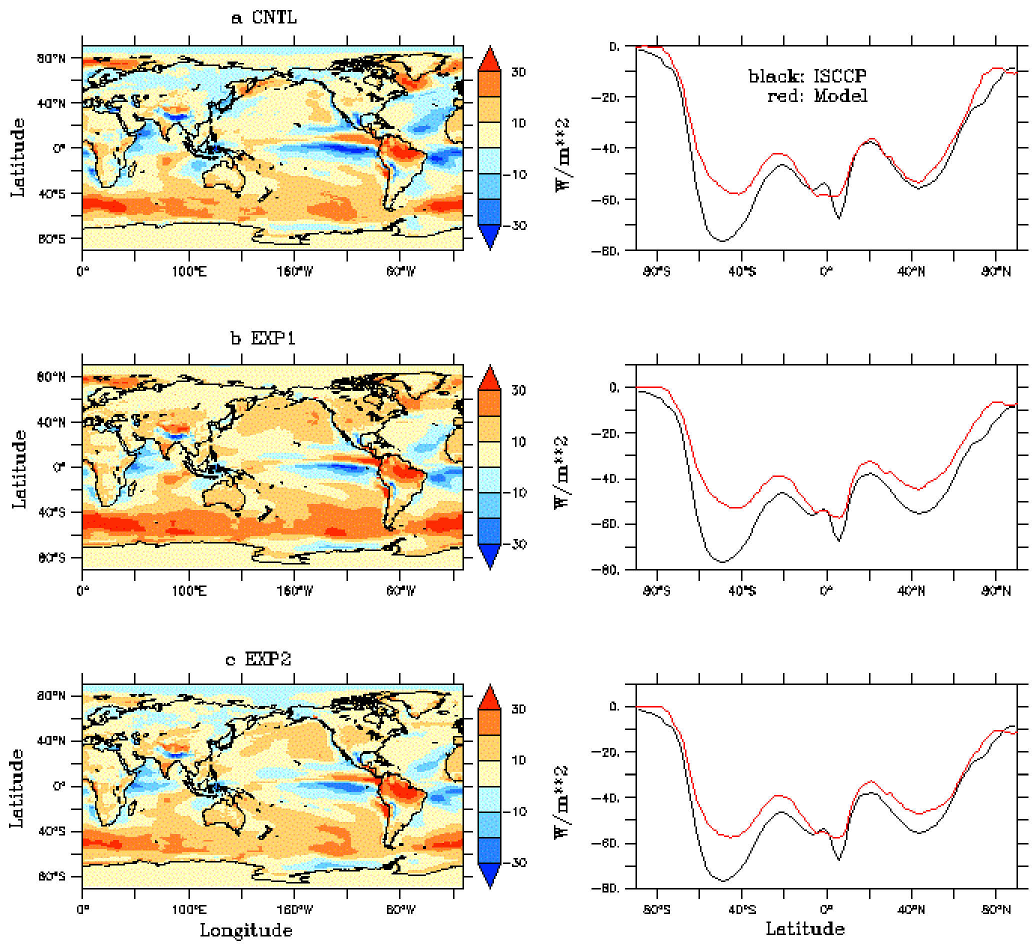

Fig. 12 Biases in cloud shortwave radiative forcing (left column) and zonal mean distribution of shortwave forcing (right) from the three ACCESS model runs. The cloud radiative forcing determined by the ISCCP-FD is used as a benchmark.

Figure 12 presents the results of shortwave cloud radiative forcing (SCRF). Over the tropical equatorial ocean, the control run (a) produces excess SCRF; this is consistent with the net solar radiation at the surface. Over the northern hemisphere, the SRF from this run is pretty good and this is very clear from the zonal mean comparison between the modelled values and ISCCP results shown in the top right panel. Using the triple clouds schemes (b) makes the SRF worse in most regions, especially over the high latitude ocean in the southern hemisphere where the SCRF is significantly underestimated. The inclusion of the modified ice cloud fraction scheme results in the simulations of SCRF improving, particular in the Northern Hemisphere. However, the improvements in the Southern Hemisphere are not large enough and the model still has a significant error over the Southern Ocean.

From the above analysis, possible problems in the PC2 cloud scheme may be revealed. The LCRF from the final ACCESS model configuration is better than the SCRF, which implies that the water cloud properties in the ACCESS model may be inaccurate. The first sign is that the low level cloud fraction is underestimated over the southern ocean, which is partially responsible for the underestimation of the SCRF and excess heat flux in this region. The second suspicion is that the cloud liquid water content predicted by the PC2 scheme may not be large enough. This underestimation can compensate for the errors due to the use of a plane parallel homogeneous cloud in a model grid box and explain why the SRF from the control run is generally better than that from the other experiments. After this uncertainty is corrected by the inhomogeneous cloud water content from the triple cloud scheme, the effect of underestimated liquid water content is exposed. The third possible problem is that the cloud phases may be incorrect over the southern ocean. Analysis of observations from satellites (Morrison *et al.* 2011) has shown the extensive presence of supercooled liquid water over the Southern Ocean region, particularly during summer, but the models may fail to predict large enough quantities of such supercooled liquid water in this region. This analysis provides a clear research target for further improving the ACCESS model in the future.

3.3 Wind stress

Wind stress has tremendous influence on SST due to its effect on the advective and diffusive processes that redistribute heat in the upper ocean. A small change in zonal wind stress can generate large anomalies in latent heat cooling, equatorial upwelling, meridional advection, and zonal advection. Among all these effects, the anomalous zonal advection contributes most to the SST anomaly in the central equatorial Pacific (Chen *et al.* 1994). Therefore, any modification to the model physics should also result in improvements to the wind stress in order to improve the SST simulation. We now check if our modifications have met this goal. Fig. 13 shows biases in the annual mean zonal wind stress due to the implementation of the Triple-cloud scheme (EXP1). Compared with the results from the control run shown in Fig. 3, the biases in zonal wind stress have been reduced in the Tropical Equatorial Ocean, northern hemispheric oceans, and the Southern Ocean between 30^o and 180^o W. The improvement over the Southern Ocean will facilitate the reduction of the warm SST biases; but the reduction of positive biases in wind stress over the tropical ocean, in principle, may not be favorable to combat cold SST biases. The cold SST biases in this region, however, have been significantly reduced from this experiment as will be shown in Fig.15. The reason for this improvement is most likely attributed to the changes in the net solar radiation at the ocean surface as shown in Fig. 7b.

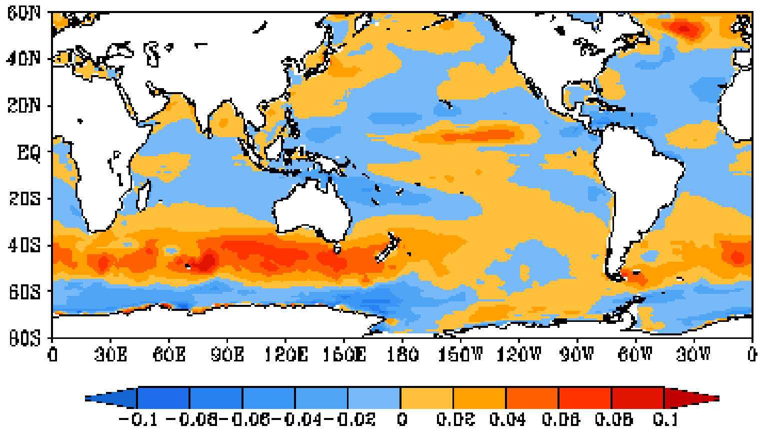

Fig. 13 Biases in annual mean zonal wind stress from EXP1 (ACCESS minus COREv2)

We further examine the effects of modifying the air-sea flux scheme on the wind stress and SST. In Fig. 14, we plot wind stress vectors from EXP2, which has included the effects of the Triple-cloud scheme and the modified PC2 ice cloud fraction scheme. The SST biases in this experiment are overlaid as colour filled contours (upper panel). We use the results from this run as a base and test the effects of modifying the air-sea flux scheme. The cold SST biases in the central Equatorial Pacific are about -2K, which may be related to the model wind stress. It has been shown in earlier studies (e.g. Chelton *et al.* 2001; Chelton 2005) that the strong SST cold tongue in the east Tropical Pacific is usually related to overly strong southeast trade winds. There is a divergence of wind stress in the middle and west Tropics that is well correlated with the maximum of the SST gradient (Chelton *et al.* 2001). Therefore, modifying the wind stress divergence will improve the SST simulation. The modification to Z_{0m} in Eq. (11) acts to ease the meridional divergence, while the modification to Z_{0s} in Eq. (12) acts to ease the southeasterly wind. Both function to reduce the surface wind stress, which can be seen in the lower panel of Fig.14 where the wind stress difference between Exp3 and Exp2 is plotted. The SST difference between these two experiments is overlaid as a background. It is seen that SST in the central equatorial Pacific from EXP3 is increased. This SST change is due to the zonal heat flux associated with the reversed surface wind stress.

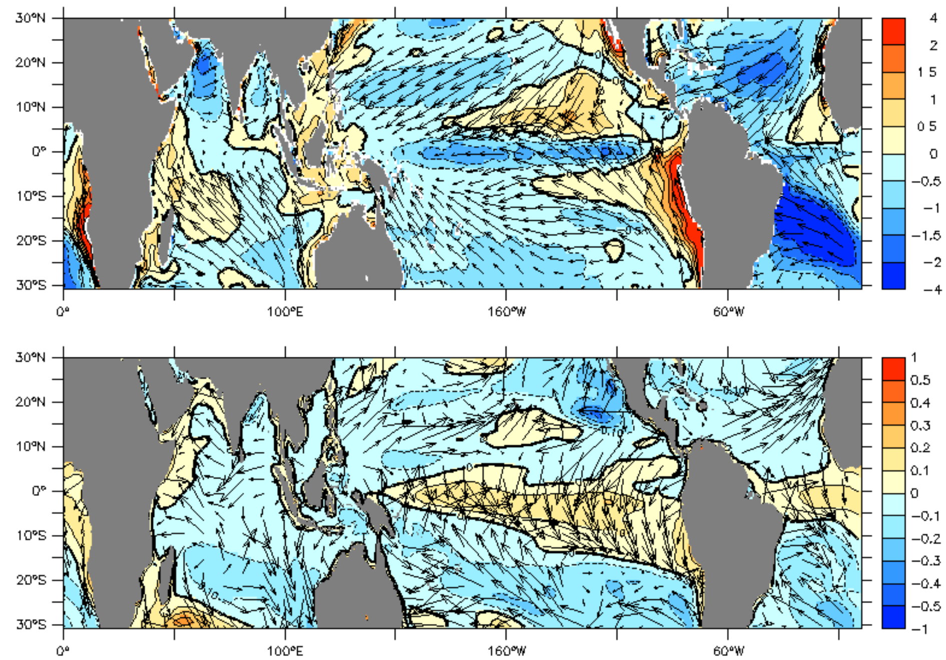

Fig. 14 Relationship between SST and surface wind stress in the Tropical Pacific Ocean. Upper panel shows wind stress with SST biases overlaid from EXP2. Lower panel shows the difference between EXP3 and EXP2 for both wind stress and SST

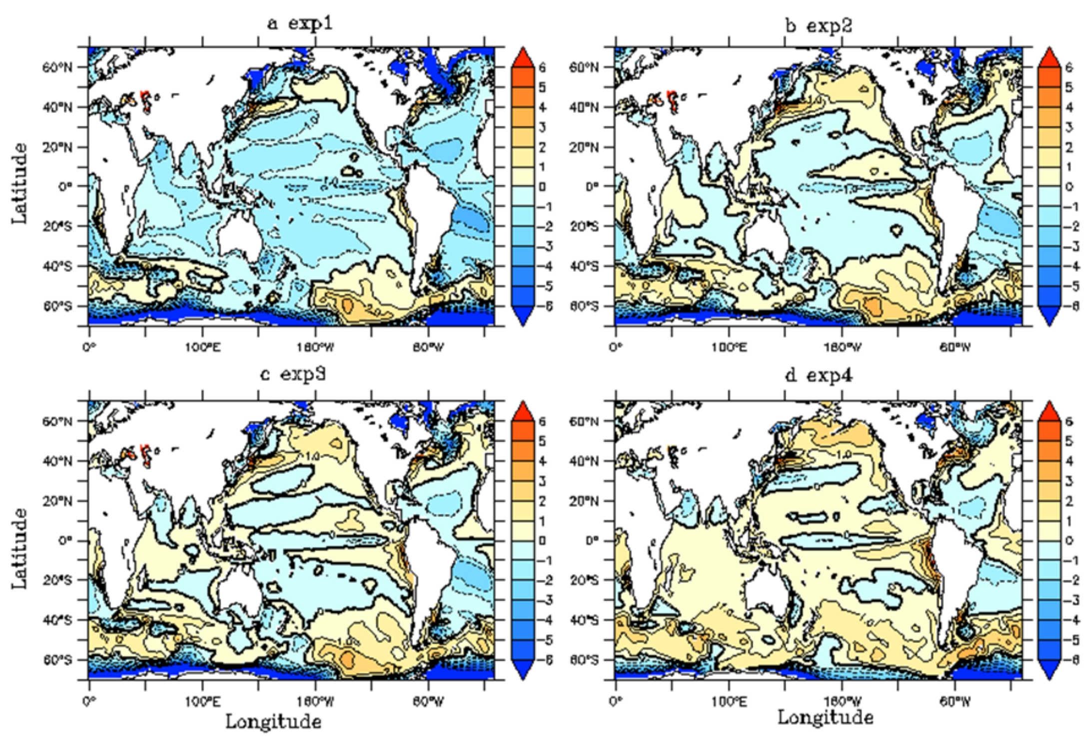

Fig. 15 SST biases simulated by ACCESS model from the four experimental runs.

3.4 SST field

Our final target is to improve the SST simulations. Figure 15 shows the distribution of SST biases from the four experimental runs. The results from the control run have been shown in Fig.1. It is seen that the implementation of the inhomogeneous cloud distribution scheme has resulted in a large improvement in the SST simulation. Cold SST biases in the northern hemisphere have been largely reduced, in particular, a large SST bias along the equatorial tropical Pacific Ocean shown in Fig. 1 has been reduced to about -2 ~ -3K in Fig. 15a. However, the negative effect from this modification is that the warm SST biases in the southern ocean are increased with the likely reasons for this discussed in the last subsection. Future research efforts will attempt to identify the reasons for this error and improve the parameterisations that contribute to the Southern Ocean SST errors. As analysed previously, the large reduction of cold SST bias in the central Equatorial Ocean is primarily due to the enhanced downward net solar radiation and this result is consistent with that presented by Chen *et al.* (1994). Implementation of the modified ice cloud fraction scheme further improves the SST simulation too. As shown in Fig. 15c, the SST cold biases are further reduced compared with that shown in Fig. 15b. It is interesting to see that this scheme not only reduces the cold biases in the middle and low latitude oceans but also reduces the warm biases in the southern high latitude ocean. Since the altitude of ice cloud in this region is much lower than that over the tropics, increases in ice cloud cover may have a cooling effect. This result supports our earlier conclusion that the cloud liquid water over the southern ocean needs increasing to combat excess solar radiation from reaching the ocean surface. Figure 15d shows the SST biases simulated by adding the modifications to the surface roughness length on top of EXP2. Although this modification has little effect on the radiation and cloud fields, it does improve the SST simulation. It can be seen that a narrow strip of the SST cold biases shown in Fig. 15c has been removed by this correction. In addition, the overall cold biases in the middle and low latitude oceans are further reduced. Figure 15e shows the changes in SST biases due to changing the vertical cloud overlap from the maximum-random to the exponential-random scheme. The SST cold biases in the Pacific and Atlantic oceans have been further reduced. The warm biases in the south-eastern Pacific are also reduced. These changes are consistent with the total cloud changes as shown in Fig. 6f. Compared with Fig. 6e, the total cloud in the sub-tropics of the Northern Pacific is increased and this increases the cold SST bias there. The total cloud amounts in the tropical Pacific and Atlantic oceans are reduced so the SST in these regions are increased. The effect of vertical cloud overlap is to change total cloud cover. We can see from this study that this change may be dependent on cloud regimes. Detailed analysis on these regimes may be necessary to understand the effect of exponential-random overlap scheme and this will be conducted in the future.

4. COMPARISON OF THE ACCESS SINGLE COLUMN MODEL IN A WEAK TEMPERATURE GRADIENT MODE TO ITS PARENT AGCM

This section presents our modification to the ACCESS SCM in order to make the simulated results from SCM more representative of those from AGCM. The conventional evaluation of single-column models (SCMs) against observations is done with large-scale vertical velocity or large-scale vertical advective tendencies specified. In this configuration there is no feedback between the model physics and large-scale dynamics. The external specification of the vertical velocity or vertical advection strongly constrains the precipitation field, and thus prevents these models from being very useful in understanding the factors which would control the occurrence or intensity of precipitation in a more realistic setting with interacting physics and dynamics. The weak temperature gradient (WTG) approximation offers a simple but physically-based way to parameterize large-scale dynamics in a SCM, allowing some interaction between physics and dynamics, although the parameterization of large-scale dynamics through the WTG is, of course, imperfect. In this work, we have attempted to test the SCM-WTG framework in a "perfect model" setting more comprehensive than has been previously used for this purpose. We have compared statistically steady solutions with a SCM run under the WTG approximation to selected tropical statistics from a simulation done with the parent GCM from which the SCM was derived. We used the HadGEM1 climate model for this purpose. We are interested in understanding the degree to which an SCM with parameterized large-scale dynamics can serve as a surrogate for the full GCM. Both successes and failures – those aspects of the GCM which the SCM can and cannot capture – are of interest.

With the free-tropospheric temperature profile taken from an RCE solution computed with the SCM over an SST of 301K, SCM-WTG has zero precipitation for SST less than 301K, with precipitation increasing with SST above that value (See Fig. 16a). This is qualitatively consistent with what has been found in similar studies with other models, both SCMs and cloud-resolving models. Above the critical SST of 301K, the SCM precipitation values are between the 50th and 75th percentile values from the GCM over similar SST. For smaller SST, the SCM-WTG underestimates the precipitation, obtaining essentially zero compared to a distribution in the GCM with significant nonzero values. Including horizontal moisture advection (Zhu and Sobel, 2011) in the SCM improves the agreement with the GCM, particularly in bringing the precipitation above zero in the lower-SST region; it also reduces the precipitation slightly for SST>301K, so that it closely matches the 50th percentile from the GCM (See Fig. 16b).

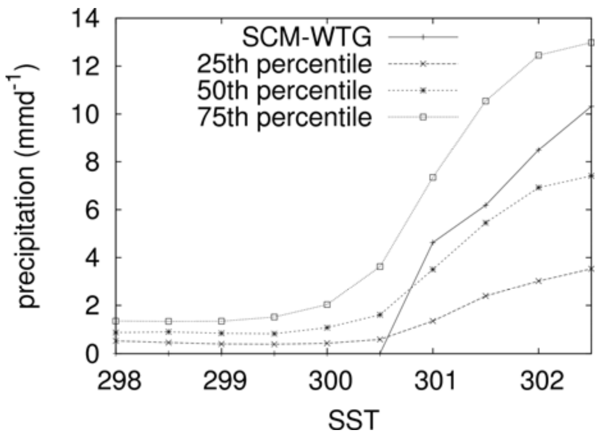

Fig. 16a Precipitation (mmd^{-1}) as a function of SST in the SCM-WTG compared to the 25th, 50th and 75th percentiles from the GCM over the Western Pacific and Indian Ocean region.

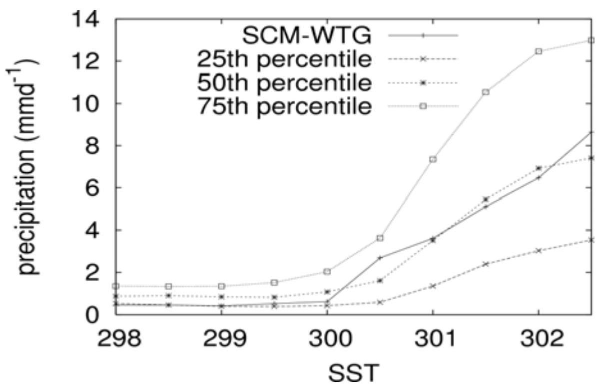

Fig. 16b Precipitation (mmd^{-1}) as a function of SST in SCM-WTG with horizontal moisture advection compared to the 25th, 50th and 75th percentile values from the GCM over the Western Pacific and Indian Ocean region.

5. IMPROVED MJO WITH CONVECTION CHANGES IN ACCESS AMIP SIMULATIONS

In Zhu and Hendon (2010), variability associated with the Madden-Julian Oscillation (MJO) in the latest version of the Met UM model is evaluated by comparison to observations and simulations from a climate- model in which a 2-dimensional cloud resolving sub-model replaced the traditional convective parameterization scheme. To better understand the cause of the poor simulation of the MJO in the Met UM, diagnosing the behaviour of convection on the model grid scale was carried out in that paper.

That work showed that in the Met UM the following features of convection associated with the MJO are not well represented: 1) There is still convection occurring in the relatively dry environment, and also the precipitation stops growing after reaching 85% of the saturation fraction value; 2) The model fails to produce the pre-moistening by shallow convection before intensive rainfall events and rapid drying after the intensive rainfall event by the meso-scale downdrafts; 3) The baroclinic nature of the zonal wind distribution associated with deep convection is not well captured, which could be due to the parameterised momentum transfer in the model; 4) The latent heat flux anomaly associated with intense rainfall events is only about half of that seen in observations and the cloud-resolved model.

To improve the simulated MJO in the ACCESS climate model, we have made two changes in the model. The first is to change the trigger for shallow convection, so that the shallow convection can happen without a vertical velocity restriction. The second is to increase the entrainment rate, which has been found useful for MJO simulation in other GCM models.

The simulation of the MJO is first assessed by examination of the space-time spectral density and signal strength of equatorially symmetric precipitation and zonal wind speed at 850 hPa U850 (symmetric latitudes 2.5-10 degree) following Hendon and Wheeler (2008). The observed spectra of rainfall (Fig. 17a) and U850 (Fig. 17b) exhibit pronounced peaks at eastward wavenumbers 1-3 (OLR) and wavenumber 1 (U850) for periods centred on about 50 d. This spectral peak is indicative of the MJO (Salby and Hendon 1994) and it is seen to be well removed and distinct from the spectral peaks associated with higher frequency Kelvin waves.

A similar analysis of the control experiment from the latest ACCESS climate model (Fig. 17c, d) reveals an absence of this strong spectral peak at 50 days, i.e., there is little MJO signal. A realistic spectrum of higher frequency Kelvin waves is simulated, but at the lower eastward frequencies associated with the MJO, the spectrum from control experiment appears mostly red, with no strong evidence of an intraseasonal spectral peak especially in OLR. Fig. 17e, f shows results from experiments in which the two changes associated with the convection scheme, noted above, are introduced. Comparing with the results from control experiment, Figs 17e, f exhibit improved spectral peak associated with the MJO in both OLR and U850, indicating that the intraseasonal variability simulation has been improved in ACCESS climate model with these convection changes.

With increasing entrainment rates, the convective detrainments rate increases as well, which helps to moisten the lower troposphere before the convection develops to the upper troposphere. Removing the restriction of vertical velocity for shallow convection allows shallow convection to happen before deep convection, and provides the pre-moistening condition for the deep convection (Zhu et. al 2009).

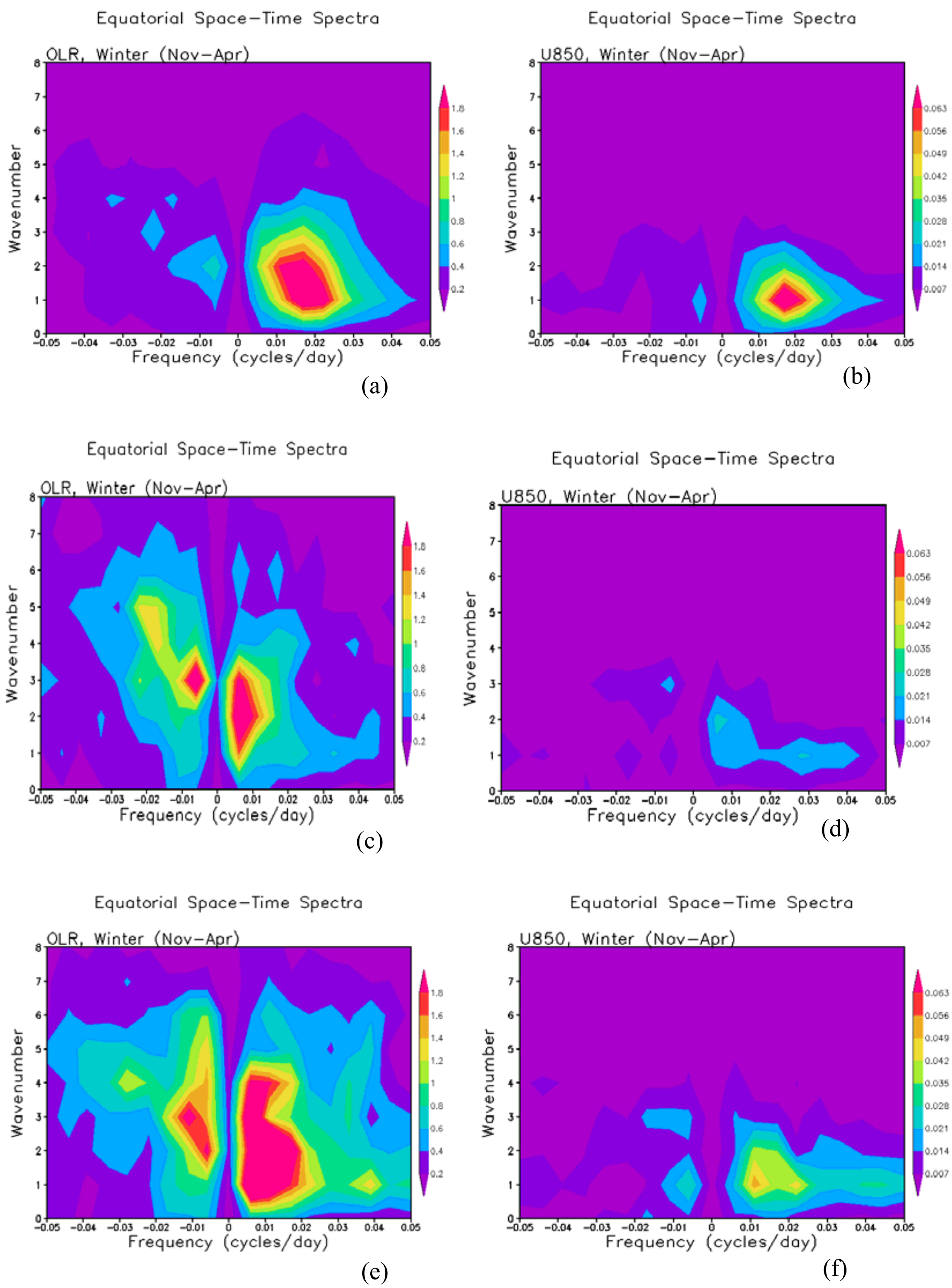

Fig. 17 Winter equatorial space-time spectra for OLR (left panel) and U850 (right panel). (a,b) are for the OBS,(c,d) are for the control experiment, and (e, f) are for the experiment with the convection changes.

6. PARAMETERIZATION OF THE STABLE BOUNDARY LAYER IN ACCESS

6.1 Background and aims

Several studies of the representation of boundary layer processes in atmospheric models have shown a number of shortcomings in the representation of the diurnal cycle (Brown *et al.* 2005; Holtslag, 2006; Svensson *et al.* 2011). Typically, the magnitude of near-surface wind speed is overestimated overnight leading to a relatively weak diurnal variability under clear skies when compared to observations. Part of this is attributable to the parameterization of stable conditions occurring overnight when wind speeds are generally light (< $2ms^{-1}$). Models that use a First Order K-profile scheme to parameterize turbulent mixing in the boundary layer apply Monin-Obukhov Similarity Theory (MOST) to calculate fluxes of heat and momentum in the surface layer, which represents approximately the lowest 10% of the boundary layer. It is recognised that MOST has some limitations at very high stabilities as it relies upon boundary layer height as a scaling term, a parameter that is difficult to define under stratified conditions (Newstadt, 1984; Smedman, 1988; Mahrt and Vickers, 2003), however it is still the most commonly used framework for the representation of surface layer fluxes in atmospheric models. Whilst still operating within MOST, it is of interest to test whether an alternate formulation of the parameterization for momentum can improve the representation of momentum transfer in the surface layer. A series of experiments was conducted with the Australian Community Climate and Earth System Simulator (ACCESS) in Single Column, Short Range Numerical Weather Prediction and coupled climate configuration to (a) test the effectiveness of an alternate stability function for momentum in improving the diurnal variability of wind speed, and (b) assess the sensitivity of the model general circulation to the change in the surface layer parameterization.

6.2 A low wind speed parameterization for stable conditions

A detailed analysis of low wind speeds under stable conditions was performed by Luhar *et al*. (2008) (hereon LH08) using field datasets from the CASES-99 intensive observational period and Cardington tower operated by the UK Met Office. The authors pointed out that turbulence continues to exist at 'super-critical' values of the gradient Richardson number ($Ri_g > 0.2 – 0.3$). The nature of this turbulence under strong stability was found to be weak and anisotropic, in agreement with the conclusions of Galperin *et al.* (2007) and Zilitinkevich et al. (2007).

Noting the scatter of observations in Fig. 18.1b, the considerable spread of wind speeds in the range $0.1 \leq \zeta \leq 2$ can be seen to fall well below that predicted by the stability functions most commonly used in models. As a result, present formulations tend to over-predict near-surface wind speed under increasingly stable conditions. As an alternate approach, LH08 proposed a switch to a new scaling function for momentum to be applied at high stabilities based on the spread of wind speed observations from the Cardington and CASES99 datasets. The rationale for this approach was:

Observations showed a marked transition between turbulent regimes in terms of anisotropy and sensible heat flux.

Wind speeds are typically overestimated in operational weather and climate models over land under stable conditions (Svensson and Holtslag, 2007).

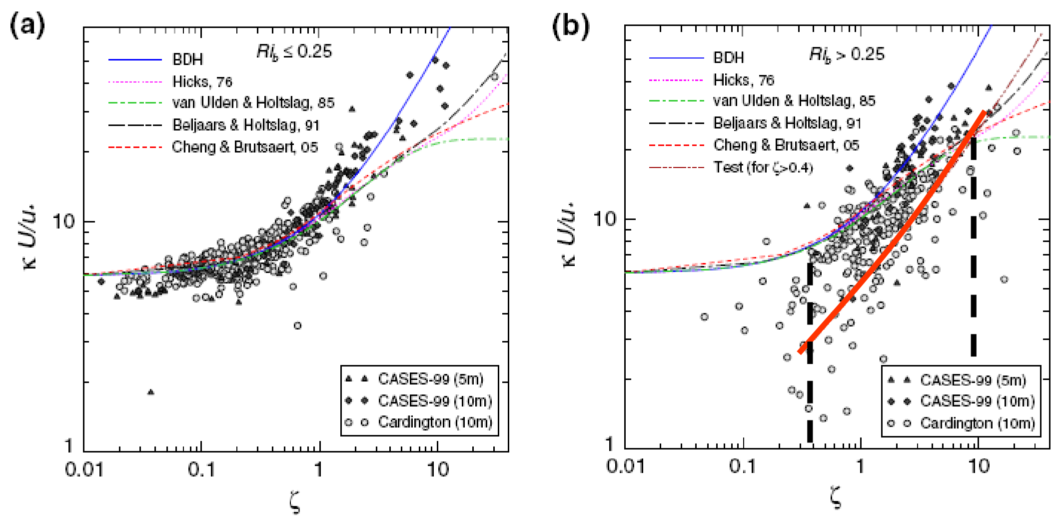

Fig. 18 Scatter of non-dimensional wind speed with stability (adapted from Luhar et al. 2008). (a) Observations for low stabilities with common momentum stability functions. (b) Observations for $Ri_B > 0.25$ with Luhar et al. (2008) momentum scaling overlaid for $0.4 \leq \zeta \leq 10$ (red).

However, rather than formulate a new flux-gradient function, the LH08 parameterization aimed to relate the non-dimensional wind speed ($\kappa U/u_*$) directly to the stability parameter ζ. The following form of the non-dimensional wind-speed was chosen and the coefficients α, β and γ were fit to observations from the Cardington tower and CASES-99. The LH08 function was:

$$\frac{\kappa \; \overline{u}}{u_*} = \alpha \left[\zeta^{\beta} \left(1 + \gamma \zeta^{1-\beta} \right) \right] \qquad (15)$$

where κ is the Von-Kármán constant, $\alpha = 1$, $\beta = 0.5$ and $\gamma = 0.3$. By defining the function in terms of dimensionless wind speed directly, one benefit of the LH08 parameterization was that it did not start with an assumption of a log-linear wind profile which is less defined at high stabilities. Furthermore, an integral form of a function fit to observations of the flux-gradient would be unable to sufficiently represent the rapid transition in turbulence character seen in the observations. However, if required the integral and gradient forms of the LH08 function may be derived easily.

6.3 Single Column Model testing

Initial test simulations showed that a 'step change' from the BH91 to the LH08 parameterization at the threshold stability of $\zeta = 0.4$ (as depicted in Fig. 18.1b) was numerically unstable. Therefore some form of smoothing needed to be applied between the two states. For this purpose a weighting function was applied, based on the cumulative normal distribution (CND):

$$f(\zeta) = \frac{1}{\sqrt{2\pi\sigma^2}} \int_{\zeta_o = 0.1}^{\zeta} \exp\left(\frac{(\zeta' - \mu)^2}{2\sigma^2}\right) \cdot d\zeta' \qquad (16)$$

This determines the area fraction under the Gaussian normal distribution between zero and 1 and may have its shape adjusted by specification of the distribution mean (μ) and standard deviation (σ). This percentage weighting is applied to both the BH91 and LH08 functions across the stability transition range. The parameterised non-dimensional wind speed, with weighted transition, is given by adding a modification to the formulation of dimensionless wind speed such that:

$$\frac{\kappa \overline{u}}{u_*} = \left[\ln\left(\frac{z}{z_o}\right) - \{\psi_{BH}(\zeta) - \psi_{BH}(\zeta_o)\} - \{\nu_L(\zeta) - \nu_L(\zeta_o)\} \right] \cdot f(\zeta) + \{\nu_L(\zeta) - \nu_L(\zeta_o)\} \qquad (17)$$

where ψ_{BH} is the BH91 integral stability function for momentum, ν_L is the LH09 non-dimensional wind speed parameterisation and $f(\zeta)$ is the smoothing function applied across the stability range $0.1 \le \zeta \le 10$.

6.4 SCM results

The smoothing of the transition between the BH91 and LH08 similarity functions proved effective in eliminating the numerical instability seen in previous experiments. A numerically stable simulation was brought about using the parameter settings of $\mu = 0.4$, $\sigma = 1.00$ in equation (16). This change to the momentum parameterization resulted in not only a decrease in nocturnal wind speed (Fig. 19a), but also had an effect on wind speeds at levels higher up in the boundary layer (Fig. 19b). Interestingly, an examination of the differences in the profiles of zonal wind speed throughout the diurnal cycles of GABLS2 revealed variations in the magnitude of this effect. At the beginning of the simulation (night 1) the LH08 parameterization had imposed a reduction in wind speed at the lowest two model levels (10m, 50m). By daybreak (08 CST), a low level jet had evolved at 120m that was considerably stronger than the BH91 simulation. This momentum quickly mixed down to the surface by early afternoon (14 CST) resulting in the entire low level profile (up to 250m) exhibiting a slightly stronger wind speed than for the equivalent time in the BH91 simulation. The profiles for BH91 and LH08 eventually became equal by evening (20 CST) as they matched a generally neutral logarithmic profile. As the boundary layer then became stable once again overnight, this pattern of profile evolution began again.

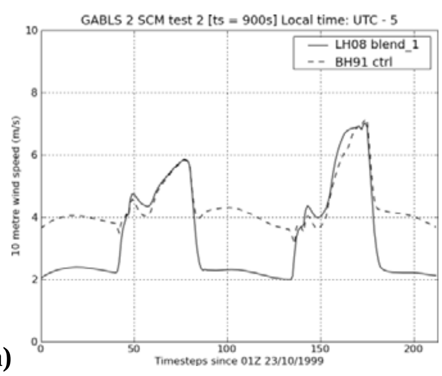

(a)

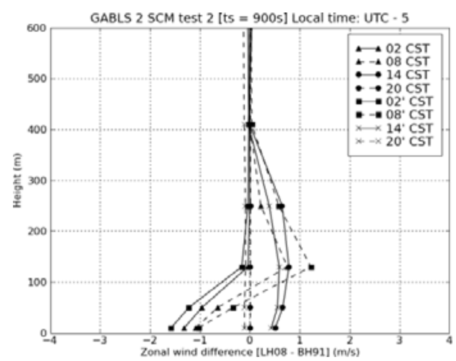

(b)

Fig. 19 Results for GABLS2 SCM test 2 (a) 10 metre wind speed, (b) difference in zonal wind profile at 6 hourly intervals (nb. prime indicates 24th Oct).

6.5 Testing in NWP forecast model

The LH08 momentum stability function in the full 3D version of the ACCESS NWP model (APS1) resulted in a noticeable increase in the diurnal range of wind speed. Under clear, stable conditions over land, wind speeds were typically decreased by between 10-20% whilst the daytime maxima remained relatively unchanged (Fig. 20a). In order to test for larger scale effects on the general circulation of the model due to the change in surface momentum, the NWP model was run for 10 days and differences noted in mean sea level pressure (MSLP) and in the tracks and life-cycles of extra-tropical cyclones. Figure 20b shows that after 6 days there are subtle changes in MSLP but these differences are very weak (< 3 hPa) and there is very little change in the structure of the circulation. The effect on the evolution of individual extra-tropical cyclones was also very weak with small decreases in system duration and pressure depth the only noticeable differences (Table 1).

Cyclone track	Control	Mod-LH08
Average duration (hrs)	95.1	90.8
Laplacian (hPa.deg^{-2})	1.42	1.56
Depth (hPa)	8.94	10.2
Radius (deg)	5.44	5.88

Table 1 Extra-tropical cyclone track statistics for 95th percentile of systems with longest duration

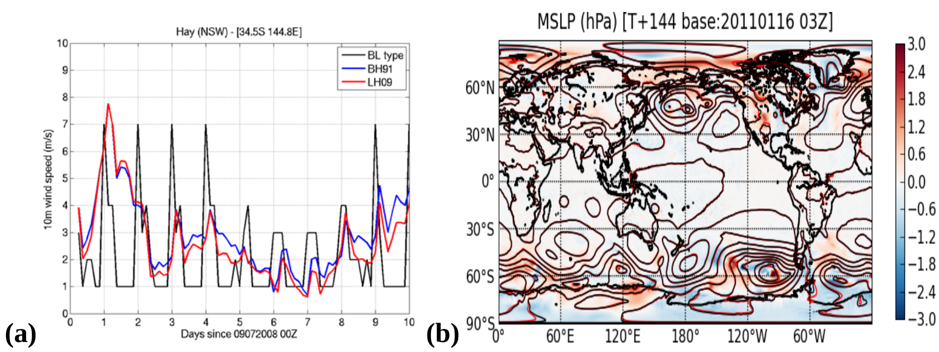

Fig. 20 (a) Time series of 10m wind speed for clear sky case for control (blue), LH08 (red). Boundary layer type indicated in black - a value of 1 denotes stable conditions. (b) Difference in day 6 ACCESS-G NWP forecast of MSLP comparing LH08 with operational momentum stability function.

6.6 Testing in coupled climate model

The LH08 low wind speed parameterization was also implemented in the ACCESS 1.3 climate model coupled to the CABLE land surface scheme, testing for effects upon the large scale circulation. The model was run for 10 years and compared to an equivalent control climatology. Overall differences to the general circulation were of little significance in response to the new parameterization. The greatest differences were noted in the surface wind speeds of the polar regions, particularly in the winter hemisphere where stable boundary layer conditions occurred most frequently (Fig. 21 a,b). However, differences were not large in magnitude and did not cause significant changes to surface fluxes of heat or moisture (typically less than 5%). This is a positive result as it indicates that the parameterization is functioning to decrease wind speeds under stable conditions and not significantly affecting the large scale climatology. The change to the parameterization of winds at the surface also has a subtle effect on wind structure of the upper atmosphere. However, as with the changes at the surface, the changes in the vertical profiles were small (< 10%). The dipolar structures of the differences indicate a subtle shift in the location of the jets, most pronounced during DJF in the southern hemisphere (note that the magnitudes of these changes are small). The effect of this could be a slight poleward shift in the storm tracks around Antarctica, however no significant change was seen in precipitation amount (not shown).

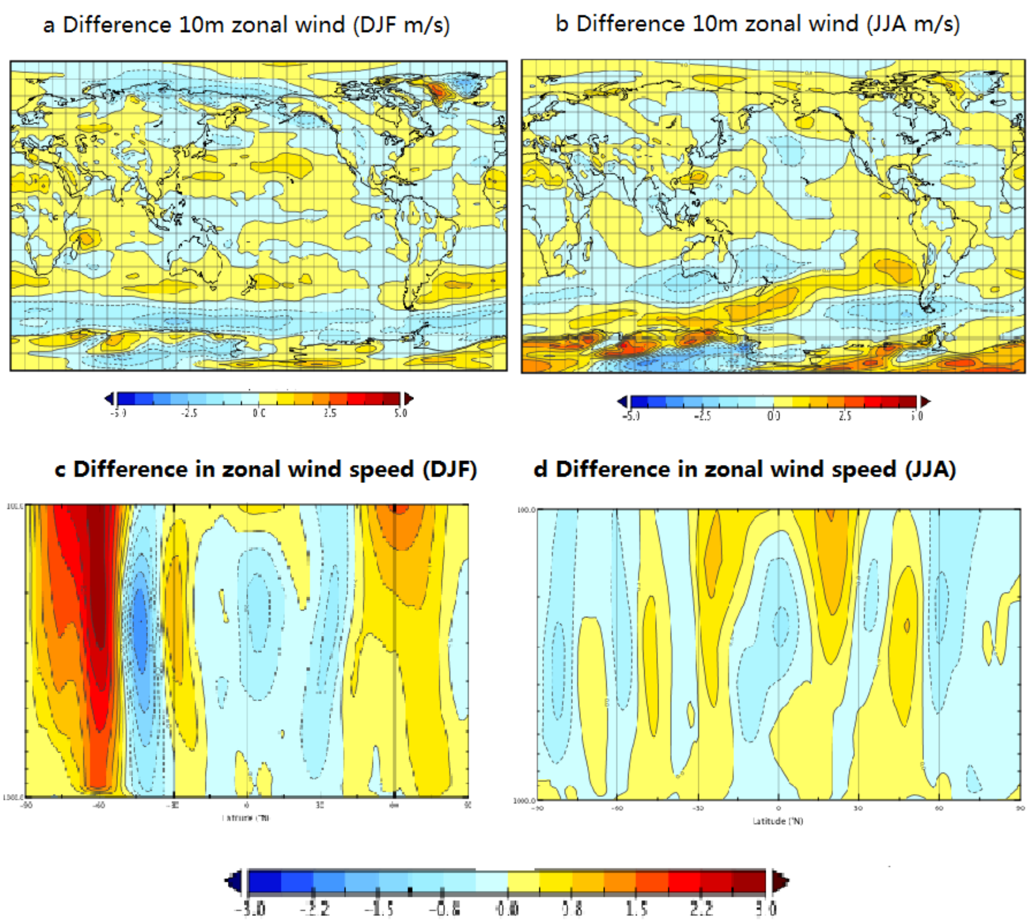

Fig. 21 ACCESS 1.3 10 year climatology difference in zonal 10m wind speed for (a) DJF and (b) JJA. Difference in zonal average zonal wind speed for (c) DJF and (d) JJA.

6.7 Summary

This series of experiments tested the sensitivity of ACCESS simulations to the LH08 stability function for momentum and demonstrated its effectiveness in decreasing near-surface wind speed under stable conditions. As a result, the model was brought more in line with case study observations of nocturnal wind speed and an improvement was seen in the magnitude of its diurnal variability. This effect upon wind speed was also seen in the full model implementation in both ACCESS NWP and coupled climate simulations (ACCESS 1.3). Importantly, ACCESS showed little sensitivity on the large scale to the change in the surface layer parameterization. On short timescales, only subtle changes were seen in the characteristics and behaviour of extra-tropical cyclones but there was a noticeable effect upon the diurnal variability of wind speed. On the longer timescales of the coupled climate model the new parameterization had a subtle effect upon wind speeds near the poles and also resulted in a very weak poleward shift in southern hemisphere jet structure during the austral summer. These experiments have shown that an improvement can be made to the representation of stable boundary layer wind speed via a relatively minor adjustment to the surface layer parameterization of momentum. Furthermore, this change appears to have no significant effect upon the large scale circulation of the model in either NWP or climate configuration making it applicable to all model configurations.

7. IMPLEMENTATION OF NAM-SCA IN ACCESS SCM AND SOME PRELIMINARY RESULTS

Cloud-convective interactions with the large-scale circulations in the tropical atmosphere are of critical importance in both global and regional modeling for both operational weather forecasts (e.g. monsoon onset) and for reliable future projections of climate change. However, the convective processes must be represented in an indirect manner, via parameterizations, due to a lack of horizontal resolution in current models, and the resulting inability of models to represent these processes explicitly. Arakawa and Shubert (1974) introduced the massflux scheme and this is the basis of most current cloud-convection representation. Progress on this problem has been slow since then e.g. Randall *et al.* (2003) suggest it is “deadlocked”.

The goal of this project is to directly address this issue by implementing a new convection scheme NAM-SCA (Nonhydrostatic Anelastic Model under the Segmentally-Constant Approximation) into the ACCESS model. The experimental setup is to implement NAM-SCA into the ACCESS SCM and then compare it with standard convective schemes during two observational case studies: GATE (Global Atmospheric Research Program's (GARP) Atlantic Tropical Experiment) Phase III and TWP--ICE (Tropical Warm Pool--International Cloud Experiment). These cases were selected both for the availability of data and the range of forcings involved: the magnitude of the large--scale forcing is ten times stronger for the TWP--ICE case than the GATE case. This implementation will then be extended to the full 3D ACCESS model.

NAM-SCA developed from studies into the subgrid-scale representation of physical processes for global models which led to a massflux convective parameterization situated between an explicit model and the standard massflux formulation (Yano *et al.* 2005, Yano and Piriou, 2008). In this scheme a full physical system is approximated by constant values (except for horizontal velocity) for every given horizontal segment – the segmentally-constant approximation (SCA).

The massflux parameterization is then obtained by assuming a nonhydrostatic anelastic model (NAM). This has been tested at Centre National de Recherches Météorologiques CNRM and Laboratoire de Météorologie Dynamique [LMD] with: limited segments, full resolution, and under dry and moist situations associated with precipitation (Yano *et al.* 2008a, b, c)

NAM-SCA can be considered as a "compressed" superparameterization. A superparameterization is a method of handling subgrid-scale physical processes by directly placing an explicit model in each grid box. The "compression" comes from the SCA and can be thought of as an extremely flexible mesh-refinement approach under a framework of finite volume. One of the main questions to address under full implementation in a 3D GCM is what degree of compression can be achieved e.g. when no convection is present, then NAM-SCA will be turned off. NAM-SCA has already demonstrated an ability to successfully simulate the Madden-Julian oscillation (MJO), which is extremely difficult to simulate with conventional parameterizations. A major Australian interest is a successful prediction of monsoon onset as well as break and active periods.

ACCESS has been described elsewhere in this paper, so only a brief discussion of the relevant schemes is mentioned here. ACCESS (Puri, 2005) is based on the U.K. Meteorological Office Unified Model (Martin *et al.* 2006). The large-scale precipitation is determined from the water or ice content of a cloud and described by Wilson and Ballard (1999). The convection scheme is based on the Gregory and Rowntree (1990) scheme, which is built on the initial buoyancy flux of a parcel of air and includes entrainment, detrainment and the evaporation of falling precipitation. The large-scale cloud is described by either the diagnostic scheme of Smith (1990) with modifications (Wilson *et al.* 2004) or a new prognostic cloud scheme (PC2, Wilson and Bushell, 2007; Wilson *et al.* 2008a), note that the ice condensate is prognostic in both schemes. A comparison of the diagnostic and prognostic cloud schemes can be found in Franklin *et al.* (2012).

7.1 NAM-SCA model formulation

The model is two-dimensional with five prognostic variables (w' vertical velocity, è potential temperature, qv water vapour, ql cloud water and p precipitating water); the horizontal velocity is the zonal wind u' and is diagnosed from the vertical velocity by mass continuity; the primes indicate that only deviations from the domain mean are considered for the two velocities; the domain mean zonal wind û is prescribed by observations; periodic boundary conditions imply the domain-mean vertical velocity vanishes, though a grid-box averaged vertical velocity is implicitly applied as part of the large-scale forcing; buoyancy is defined by the virtual potential-temperature; all physical variables are horizontally advected by the total zonal wind û + u'; the reference state potential temperature and water vapour is defined by domain-averaged vertical profiles that are updated every host-model timestep ÄT, which is 20 minutes for the ACCESS SCM.

The large-scale/convective scale coupling is via a prognostic equation for any physical quantity ö i.e.

$$\frac{\partial \varphi}{\partial t} = -\left[\frac{\partial}{\partial x}\left(u' + \overline{u}\right)\varphi + \frac{1}{\rho}\frac{\partial}{\partial z}\rho w' \varphi\right] + F_c + F_L \qquad (18)$$

Where ñ is density while F_c and F_L are tendencies for convective-scale processes in NAM-SCA and large-scale processes in the host model ACCESS, respectively. Now, while F_L is made up of large-scale advection and physical processes (radiation, surface fluxes, etc) we estimate it by

$$F_L = \frac{\overline{\varphi}*\left(t + \Delta T\right) - \overline{\varphi}\left(t\right)}{\Delta T} \qquad (19)$$

Where ö*(t+ÄT) is the latest state for ö before NAM-SCA is called. Thus, NAM-SCA is integrated in time from t to t+ÄT with both the large-scale zonal wind û and forcing F_L fixed, and then the last state ö*(t+ÄT) is copied to ACCESS as an update of the domain-averaged/grid-box mean quantity. This is done for the five prognostic variables (w', è, qv, ql and p) as well as for the mean cloud fraction over the period ÄT. Note that NAM-SCA at present only has liquid miscrophysics, so following Grabowski (1998) the cloud water is re-interpreted as a mixture of liquid and ice depending on the temperature: above -5^{o}C all liquid; below -20^{o}C all ice; and between -5^{o}C and -20^{o}C a linearly interpolated mixing ratio is used.

7.2 NAM-SCA preliminary results

We have been testing NAM--SCA performance by varying both its minimum horizontal model resolution, Δx, and the horizontal domain size, L, for ranges of Δx = 0.5-16km and L = 32-512km.

Preliminary results suggest that improved simulations do not automatically occur as the domain size and model resolutions are increased, which one would intuitively expect. An example of this counter-intuitive result can be seen in Fig. 22. Here the mixing ratio for the TWP-ICE simulation with Δx=16km and L=256km is plotted over the height range ~3-11km in Fig. 2(d). Figs 22(a)-(c) plot the difference from this for the simulations with the same L but Δx=8km, 4km and 2km, respectively.

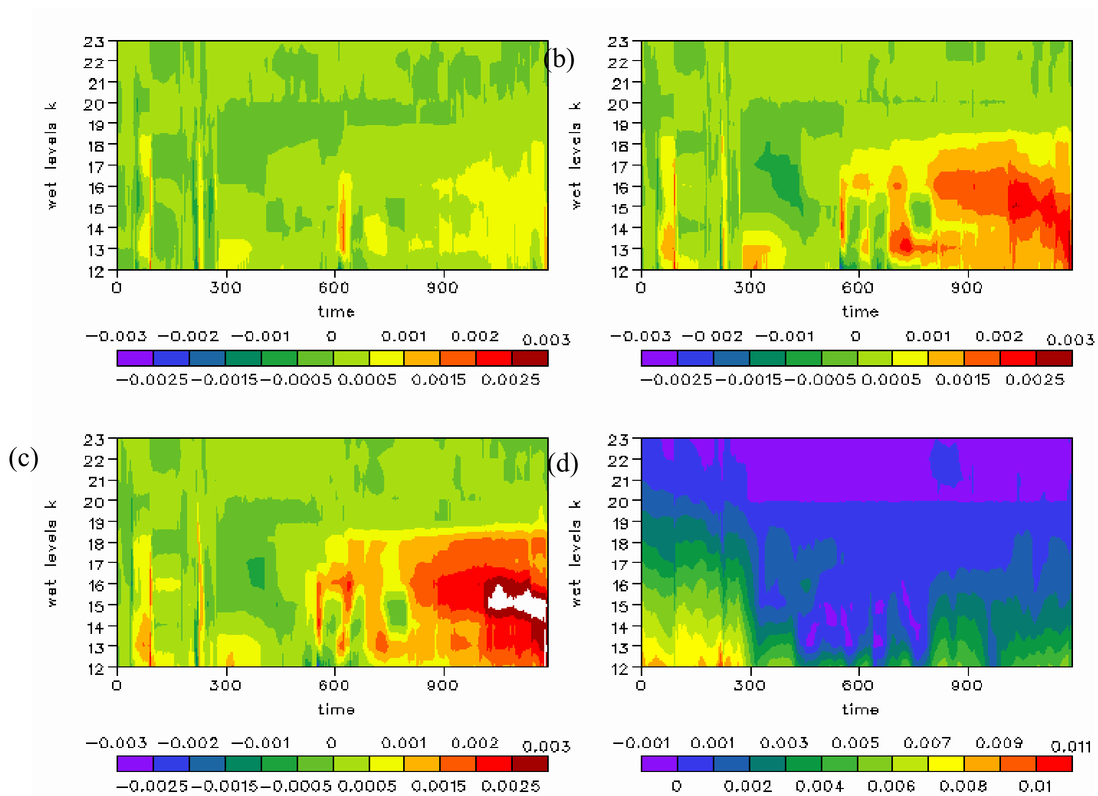

Fig. 22 Time (ACCESS timesteps=20min)/model level (from ~3km to ~11km) plot of (d) mixing ratio for the TWP-ICE case from the Δx=16km simulation. (a)-(c) are plots of differences from this for Δx=8km, 4km and 2km. All are run over a NAM-SCA horizontal domain of L=256km.

Here we see that as the NAM-SCA resolution increases we get an increased moistening after mid-way through the runs, time=600. But contrary to this near time=300 we see that Δx=4km has the largest drying/moistening dipole between levels 17 and 12. So simply increasing the resolution does not lead to consistent changes in the simulations.

This point is again demonstrated in Fig. 23 where the outgoing longwave radiation is plotted for TWP-ICE with Δx=16, 8, 4 and 2 km. Once more we do not see a consistent relationship between the NAM-SCA resolution used and the changes in a physical quantity. For example, near time=300, the two lowest resolution simulations Δx=16 and 8km (black and red lines) are most similar with low values (~110-115 Wm^{-2})while the two highest resolution runs Δx=4 and 2km (green and blue lines) have similar much high values (~140-160Wm^{-2}). However later around time=800 we see that all have similar values, though Δx=16 and 2km are most similar, as are Δx=8 and 4km. Thus, it would seem that depending on the atmospheric situation the resolution can vary between having a large impact or almost none, and not necessarily in a consistent way related to increasing resolution.

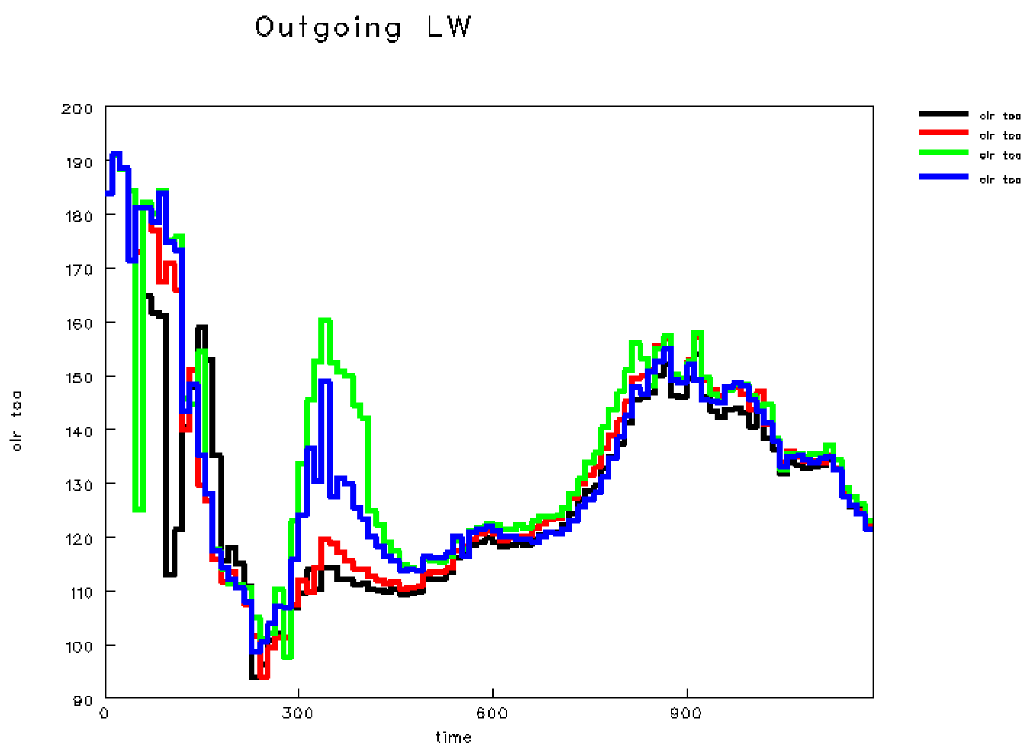

Fig. 23 Outgoing longwave radiation (Wm^{-2}) against ACCESS timestep for TWP-ICE simulations using a horizontal domain L=256km and Δx=16, 8, 4 and 2km (black, red, green and blue lines, respectively)

A similar implementation of NAM-SCA has been made in ECHAM (ECMWF [European Centre for Medium Range Weather Forecasts] Hamburg version Atmospheric Model) and results from this are compared to those from ACCESS and reported in a collaborative paper which has been submitted (Yano *et al.* 2012).

The preliminary results discussed here are under further investigation on two fronts: to examine the “grey area” in models where the need for parameterizations drops off as the resolution increases to such an extent that physical processes (such as convection) start to be resolved; and to investigate the impact of NAM-SCA when we introduce it to the ACCESS 3D model. One possible, longer-term, goal, would be the use of NAM-SCA as a cloud-resolving “truth” in evaluating how the model represents convection as it occurs within the MJO, and how the convective parameterization can be subsequently improved.

8. SUMMARY AND CONCLUSIONS

In this report, the major modifications to the MetUM atmospheric physics have been documented. These include the modifications to the UM model cloud, radiation and ocean surface stress fields for improving the ACCESS coupled-model simulation, the modification to the convection scheme for improving the ACCESS model MJO simulation, the modification to boundary scheme for improving low level wind speed simulation and implementation and test of a superparameterized cloud scheme in ACCESS SCM.

The initial ACCESS coupled-model had a significant cold SST bias in the tropical equatorial region. Our studies have shown that this SST cold bias was largely due to the incorrect representation of model clouds and partially due to the ocean surface stress parameterization. The initial version of the ACCESS model assumed a plane-parallel homogeneous cloud distribution, and this blocks more solar radiation from reaching the tropical ocean than a more realistic cloud distribution. The model does not produce enough high level clouds in the tropics and therefore allows more longwave radiation to escape out of the Earth's atmosphere. Both deficiencies cause a cooling effect at the ocean surface. To solve these problems we implemented a horizontal inhomogeneous cloud scheme in the radiation calculations, which led to a significant improvement in the SST simulation. We further modified the ice cloud fraction parameterization, which led to significant improvements in the modeled cloud amounts and cloud radiative forcing. This scheme also improved the SST simulation. Our third modification was to replace the vertical cloud overlap method by an exponential-random overlap scheme, which again improved the SST simulation. The fourth modification was to improve the surface stress modeling. The impact of this modification also reduced the cold SST biases. All these modifications have been used in the ACCESS1.3 IPCC AR5 and CMIP5 experiments with the exception of the exponential-random overlap scheme which was tested after those experiments had been submitted.

The SCM with large-scale dynamics parameterized by the adoption of the weak-temperature-gradient approximation, has proved to be able to capture the relationship between model physics and the boundary forcings in a GCM. It thus provides a useful tool to test the impact of model physics changes on climate model simulations, whilst retaining the advantages (simplicity, efficiency, etc) of the SCM framework.

The convective-parameterization sensitivity studies presented here demonstrate the potential for improvement of the simulated MJO in the ACCESS climate model. Future work will further investigate the moistening effects of changes to the shallow convection scheme and entrainment rates, and examine the impact on the model simulation in more detail. The ultimate goal is to be able to identify a set of convection scheme improvements which best reduce model biases and enhance MJO simulation.

Changes in the stability function for momentum used in ACCESS proved effective in reducing the overprediction of near-surface wind speed under stable conditions. Tests across a range of model configurations showed little sensitivity on the large scale to the change in the surface layer parameterization. On both short and longer timescales, no significant changes were seen in the distribution of wind speed or storm track behaviour but there was a noticeable effect upon the diurnal variability of wind speed in regions commonly experiencing stable conditions.

ACCESS, along with most current atmospheric models, must represent convective processes in an indirect manner, via parameterizations, and not explicitly due to a lack of horizontal resolution. However resolution is increasing, particularly in NWP and limited area models, and the question of when convective parameterizations should be "turned off" because the model can explicitly resolve some physical quantities is coming to the fore. In order to examine this issue we have successfully implemented the NAM-SCA convective superparameterization scheme into the ACCESS SCM and preliminary results suggest that improved simulations do not automatically occur as the domain size and model resolutions are increased. Future work in this area will be to implement NAM-SCA into the ACCESS 3D model and to examine the "grey area" where parameterizations and explicit resolution in models intersect.

REFERENCES

Arakawa, A. and Shubert, W.H. 1974, Interaction of a cumulus cloud ensemble with the large-scale environment Part I. *J. Atmos. Sci*., **31**, 674-701.

Barker, H.W. and Davies, J.A. 1992. Solar radiative fluxes for stochastic, scale-invariant broken cloud fields. *J. Atmos. Sci.* **49**: 1115–1126.

Barker, H.W., Stephens, G.L. and Fu, Q. 1999. The sensitivity of domain-averaged solar fluxes to assumptions about cloud geometry. *Q. J. R. Meteorol. Soc.* **125**: 2127–2152.

Bi, D., Dix, M., Marsland, S.J., O'Farrell, S., Rashid, H., Uotila, P., Hirst, A.C., Kowalczyk, E., Golebiewski, M., Sullivan, A., Yan, H., Hanna, N., Franklin, C., Sun, Z., Vohralik, P., Watterson, I., Zhou, X., Fiedler, R., Collier, M., Ma, Y., Noonan, J., Stevens, L., Uhe, P., Zhu, H., Griffies, S. M., Hill, R., Harris, C. and Puri, K. 2013a. The ACCESS Coupled Model: Description, Control Climate and Evaluation. *Aust. Met. Oceanog. J*. 62,4.

Bi, D., Marsland, S.J., Uotila, P., O'Farrell, S., Fielder, R., Sullivan, A., Griffies, S.M., Zhou, X. and Hirst, A.C. 2013b. ACCESS OM, the Ocean-Sea Ice Core of the ACCESS Coupled Model. *Aust. Met. Oceanog. J.*, 62,4.

Bodas-Salcedo, A., Ringer, M.A. and Jones, A. 2008. Evaluation of the surface radiation budget in the atmospheric component of the Hadley Centre Global Environmental Model (HadGEM1). *J. Climate*, 21, 4723-4748, doi:10.1175/2008JCLI2097.1.

Bodas-Salcedo, A., Williams, K., Field, P. and Lock, A. 2012. The surface downwelling solar radiation surplus over the Southern Ocean in the Met Office model: the role of midlatitude cyclone clouds. *J. Climate*, doi:10.1175/JCLI-D-11-00702.1, in press.

Boutle, I.A. and Morcrette, C.J. (2010). Parametrization of area cloud fraction. *Atmos. Sci. Let.* **11**: 283–289, **DOI:** 10.1002/asl.293

Brown, A.R., Beljaars, A.C.M., Hersbach, H., Hollingsworth, A., Miller, M. and Vasiljevic, D. 2005: Wind turning across the marine atmospheric boundary layer, *Quart. Journ. Roy. Met. Soc*., **131**, 1233-1250.

Carlin, B., Fu, Q., Lohmann, U., Mace, G.G., Sassen, K. and Comstock, J.M. 2002. High-cloud horizontal inhomogeneity and solar albedo bias.

Chen, D., Busalacchi, A.J. and Rothstein, L.M. 1994. The roles of vertical mixing, solar radiation,and wind stress in a model simulation of the sea surface temperature seasonal cycle in the tropical Pacific Ocean. *J. Geophys. Res*., 99, C10, 20345-20359.

Chelton, D.B., Esbensen, S.K., Schlax, M.G., Thum, N. and Freilich, M.H. 2001. Observations of coupling between surface wind stress and sea surface temperature in the Eastern Tropical Pacific. *J. Climate,* 14, 1479-1498.

Chelton, D. 2005. The impact of SST specification on ECMWF surface wind stress fields in the Eastern Tropical Pacific. *J. Climate*, 18, 530-550.

Chevallier, F., Kelly, G., Simmons, A.J., Uppala, S. and Hernandez, A. (2004) High Clouds over Oceans in the ECMWF 15- and 45-Yr Reanalyses. *J. Climate*, 18, 2647-2661.

Davies, T., Cullen, M.J.P., Malcolm, A.J., Mawson, M.H., Staniforth, A., White, A.A. and Wood, N. 2005: A new dynamical core for the Met Office's global and regional modelling of the atmosphere. *Quart. J. Roy. Meteor. Soc*., 131, 1759–1782.

Fairall, C.W., Bradley, E.F., Hare, J.E., Grachev, A.A. and Edson, J.B. 2003: Bulk Parameterization of Air–Sea Fluxes: Updates and Verification for the COARE Algorithm. *J. Climate*, **16**, 571–591.

Franklin, C.N., Sun, Z., Bi, D., Dix, M., Yan, H. and Bodas-Salcedo, A. 2013, Evaluation of clouds in ACCESS using the satellite simulator package COSP. Part I: Global, seasonal and regional cloud properties. *J. Geophy. Res*. 118, 723-748, DOI: 10.1029/2012JD018469

Franklin, C.N., Jakob, C., Dix, M., Protat, A. and Roff, G. 2012. Assessing the performance of a prognostic and a diagnostic cloud scheme using single column model simulations of TWP–ICE. *Q. J. R. Meteorol. Soc.* **138**: 734–754. DOI:10.1002/qj.954

Galperin, B., Sukoriansky, S. and Anderson, P.S. 2007: On the critical Richardson number is stably stratified turbulence, *Atm. Sci. Lett.*, **8**, 65-69.

Geleyn, J.F. and Hollingsworth, A. 1979. An economical, analytical method for the computation of the interaction between scattering and line absorption of radiation. *Contrib. Atmos. Phys.* **52**: 1–16.

Grabowski, W.W. 1998, Towards cloud resolving modeling of large-scale tropical circulations: A simple cloud microphysics parameterization. *J. Atmos. Sci*., **55**, 3283-3298.

Gregory, D. and Rowntree, P.R. 1990. A mass flux convection scheme with representation of cloud ensemble characteristics and stability-dependent closure. *Mon. Wea. Rev.*, ***118***, 1483-1506.

Gregory, J. 1999. Representation of the Radiative Effects of ConvectiveAnvils. Hadley Centre Technical Note 7, Met. Office: Exeter, UK.

Griffies, S.M. 2009: Elements of MOM4p1: GFDL *Ocean Group Tech. Rep. No. 6*, NOAA/Geophysical 989 Fluid Dynamics Laboratory, 444 pp

Haynes, J.M., Christian, J., Rossow, W.B., Tselioudis, G. and Brown, J. 2011, Major Characteristics of Southern Ocean Cloud Regimes and Their Effects on the Energy Budget

Hendon, H.H. and Wheeler, M.C. 2008: Some space-time spectral analyses of tropical convection and planetary-scale waves, *Journal of the Atmospheric Sciences*, ***65***, 2936-2948.

Hewitt, H.T., Copsey, D., Culverwell, I.D., Harris, C.M., Hill, R.S.R., Keen, A.B., McLaren, A.J. and Hunke, E.C. 2011: Design and implementation of the infrastructure of HadGEM3: the next-generation Met Office climate modelling system. *Geosci. Model Dev*., **4**, 223–253, doi:10.5194/gmd-4-223-2011.

Hogan, R.J. and Illingworth, A.J. 2000. Deriving cloud overlap statistics from radar. *Q. J. R. Meteorol. Soc.* **126**: 2903–2909.

Holtslag, A.A.M. 2006: GEWEX Atmospheric Boundary-Layer Study (GABLS) on stable boundary layers, *Boundary-Layer Meteorol*., **118**, 243-246.

Hunke, E.C. and Lipscomb, W.H. 2010: CICE: The Los Alamos sea ice model documentation and 1011 software user's manual, Version 4.1, LA-CC-06-012, Los Alamos National Laboratory, N.M., 1012 76 pp.

Jungclaus, J.H. and Co-authors, 2006: Ocean Circulation and Tropical Variability in the Coupled Model ECHAM5/MPI-OM. *J. Climate*, **19**, 3952–3972.

Kowalczyk, E.A., Wang, Y.P., Law, R.M., Davies, H.L., McGregor, J.L. and Abramowitz, G. (2006): The CSIRO Atmosphere Biosphere Land Exchange (CABLE) model for use in climate models and as an offline model. CSIRO Marine and Atmospheric Research paper 013, www.cmar.csiro.au/e-print/open/kowalczykea_2006a.pdf

Large, W.G. and Yeager, S. 2008. The global climatology of an interannually varying air-sea flux data set. *Climate Dynamics*, DOI 10.1007/s00382-008-0441-3.

Large, W. and Yeager, S. 2004. Diurnal to decadal global forcing for ocean and sea ice models: the data sets and flux climatologies. CGD Division of the National Center for Atmospheric Research, NCAR Technical Note: NCAR/TN-460+STR.

Lin, J-L. 2007: The Double-ITCZ Problem in IPCC AR4 Coupled GCMs: Ocean–Atmosphere Feedback Analysis. *J. Climate*, 20, 4497–4525.

Luhar, A.K., Hurley, P.J. and Rayner, K.N. 2008: Modelling near-surface low winds over land under stable conditions: Sensitivity tests, flux-gradient relationships, and stability parameters, *Boundary-Layer Meteorol*., **130**, 249-274.

Luo, J-J., Masson, S., Roeckner, E., Madec, G. and Yamagata, T. 2005: Reducing Climatology Bias in an Ocean–Atmosphere CGCM with Improved Coupling Physics. *J. Climate*, **18**, 2344–2360.

Ma, Y., Zhou, X., Bi, D., Sun, Z. and Hirst, A.C. (2012). Improved Air-Sea Flux Algorithms in Ocean-Atmospheric Coupled Model for Projection of Global Ocean SST and its Tropical Pacific Variability. *Submitted to J. Climate.*

Madec, G. (2008). NEMO ocean engine, note du pole de mod´elisation. Institut Pierre-Simon Laplace (IPSL), Paris, France, (27). ISSN No 1288-1619

Mahrt, L. and Vickers, D. 2003: Formulation of turbulent fluxes in the stable boundary layer, *Journ. Atmos. Sci*., **60**, 2538-2548.

Martin, G.M., Ringer, M.A., Pope, V.D., Jones, A., Dearden, C. and Hinton, T.J. (2006), The physical properties of the atmosphere in the new Hadley Centre Global Environmental Model (HadGEM1). Part I: Model description and global climatology, *J. Climate*., **19**, 1274-1301.

Martin, G.M., Milton, S.F., Senior, C.A., Brooks, M.E., Ineson, S., Reichler, T. and Kim, J. 2010: Analysis and Reduction of Systematic Errors through a Seamless Approach to Modelling Weather and Climate. *J. Climate*, 23, 5933–5957, doi:10.1175/2010JCLI3541.1.

Morrison, A.E., Siems, S.T. and Manton, M.J. 2011: A Three-Year Climatology of Cloud-Top Phase over the Southern Ocean and North Pacific. *J. Climate*, **24**, 2405–2418. doi: http://dx.doi.org/10.1175/2010JCLI3842.1

Niewstadt, F.T.M. 1984: The turbulent structure of the stable, nocturnal boundary layer, *Journ. Atmos. Sci*., **41**, 2202-2216.

Puri, K. 2005, Project Plan for ACCESS, http://www.accessimulator.org.au/report/index.html

Puri, K. and co-authors, 2010: Preliminary results from Numerical Weather Prediction implementation of ACCESS, *CAWCR Research Letters Issue 5, December 2010,* 15-22

Randall, D.A., Coakley Jr, J.A., Fairall, C.W., Kropfli, R.A. and Lenschow, D.H. 1984. Outlook for research on sub-tropical marine stratiform clouds. *Bull. Amer. Meteorol. Soc.* **65**: 1290–1301.

Randall, D.A., Khairoutdinov, M., Arakawa, A. and Grabowski, W. 2003, Breaking the cloud parameterization deadlock, *Bull. Amer. Soc*., **84**, 1547-1564.

Rossow, W.B., Walker, A.W. and Garder, L.C. (1993). Comparison of ISCCP and other cloud amounts. *J. Climate*, 6, 2394-2418.

Salby, M.L. and Hendon, H.H. 1994: Intraseasonal behaviour of winds, temperature and convection in the tropics. *J. Atmos. Sci.,* **51**, 2207-2224.

Shinoda, T. 2005: Impact of the Diurnal Cycle of Solar Radiation on Intraseasonal SST Variability in the Western Equatorial Pacific. *J. Climate*, **18**, 2628–2636. doi: http://dx.doi.org/10.1175/JCLI3432.1

Shonk J.K.P., Hogan, R.J., Mace, G.G. and Edwards, J.M. (2010). Effect of improving representation of horizontal and vertical cloud structure on the earth's global radiation budget. Part I: review and parameterization. *Q. J. R. Meteorol. Soc.* 136 (1), 191-204.

Slingo, A. 1990. Sensitivity of the Earth's radiation budget to changes in low clouds. *Nature* **343**: 49–51.

Smedman, A-S. 1988: Observations of a multi-level turbulence structure in a very stable atmospheric boundary layer, *Boundary-Layer Meteorol*., **44**, 231-253.

Smith, R.N.B. 1990. A scheme for predicting layer clouds and their water contents in a general circulation model. *Q. J. R. Meteorol. Soc.* **116**: 435–460.

Steeneveld, G.J., Van De Wiel, B.J.H. and Holtslag, A.A.M. 2006: Modeling the evolution of the atmospheric boundary layer coupled to the land surface for three contrasting nights in CASES-99, *Journ. Atm. Sci*., **63**, 920-935.

Svensson, G. and Holtslag, B. 2007: The diurnal cycle – GABLS second intercomparison project. *GEWEX News*, **17** (1), 9-10.

Svensson G., et al. 2011: Evaluation of the diurnal cycle in the atmospheric boundary layer over land as represented by a variety of Single-Column Models: The second GABLS experiment, *Boundary-Layer Meteorol*., **140**, 177-206.

Taylor, K.E., Stouffer, R.J. and Meehl, G.A. 2012: An Overview of CMIP5 and the experiment design. *Bull. Amer. Meteor. Soc.*, **93**, doi:10.1175/BAMS-D-11-00094.1.

Trenberth, K.E. and Fasullo, J.T. 2010. Simulation of present-day and twenty-first-centure energy budgets of the southern oceans. *J. Climate*, 23 (2), 440-454, doi:10.1175/2009JCLI3152.1.

Valcke, S. 2006. OASIS3 User Guide. PRISM-Support Initiative, Report No. 3, 64pp.

Wild, M. 2005,Solar radiation budgets in atmospheric model intercomparisons from a surface perspective. *Geophys. Res. Lett.*, 32, doi:10.1029/2005GL022421.

Wilson, D., Smith, R.N.B., Gregory, D., Wilson, C., Bushell, A.C. and Cusack, S. 2004. Unified Model documentation paper 26. The large-scale cloud scheme and saturated specific humidity. Available from Met Office.

Wilson, D, and Bushell A. 2007. *Annexe to Unified Model Documentation paper 29. The PC2 Cloud Ccheme*. Met Office: Exeter, UK.

Wilson, D., Smith, R.N.B., Gregory, D., Wilson, C., Bushell, A.C. and Cusack, S. 2004. *Unified Model Documentation Paper 26. The Large-Scale Cloud Scheme and Saturated Specific Humidity*. Met Office: Exeter, UK.

Wilson, D.R., Smith, R.N.B., Gregory, D., Wilson, C.A., Bushell, A.C. and Cusack, S. 2007. The large-scale cloud scheme and saturated specific humidity. *Unified Model Documentation Paper* **29**: 14–16.

Wilson, D.R., Bushell, A.C., Kerr-Munslow, A.M., Price, D. and Morcrette, C. 2008a. PC2: A prognostic cloud fraction and condensation scheme. Part I: Scheme description. *Q. J. R. Meteorol. Soc.* **134**: 2093–2107.

Wilson, D.R., Bushell, A.C., Kerr-Munslow, A.M., Price, D., Morcrette, C. and Bodas-Salcedo A. 2008b. PC2: A prognostic cloud fraction and condensation scheme. Part II: Results of climate model simulations. *Q. J. R. Meteorol. Soc.* **134**: 2109–2125.

Walters, D. N., and co-authors (2011). The Met Office Unified Model Global Atmosphere 3.0/3.1 and JULES Global Land 3.0/3.1 configurations. *Geosci. Model Dev.*, 4, 919–941. DOI:10.5194/gmd-4-919-2011.

Wu, X. and Liang, X. 2005. Radiative effects of cloud horizontal inhomogeneity and vertical overlap identified from a month-long cloud-resolving model simulation. *J. Atmos. Sci.* **62**: 4105–4112.

Yano, J.-I., Cheedela, S.K. and Roff, G.L. 2012, A compressed super-parameterization: Test of NAM-SCA under single-column GCM Configurations, Submitted to *Atmospheric Chemistry and Physics*, 26 June 2012.

Yano, J.-I., Redelsperger, J.-L., Guichard, F. and Bechtold, P. 2005, Model decomposition as a methodology for developing convective-scale representations in global models, *Quat. J. Roy. Met. Soc.*, **131**, 2313-2336.

Yano, J.-I. and Pirou, J.M. 2008, A hierarchy of subgrid-scale convective schemes: from the cloud-resolving model to the standard massflux parameterization, *submitted to J. Atmos. Sci*.

Yano, J.-I., Bernardet, P., Benard, P. and Lahellec, A. 2008a, NAM-SCA: Nonhydrostatic Anelastic Model under Segmentally-Constant Approximation: I. Dry formulation and a phase-spcae investigation of the single plume dynamics, *submitted to Mon. Wea. Rev*.

Yano, J.-I., Bernardet, P., Benard, P., Couvreux, F. and Lahellec, A. 2008b, NAM-SCA: Nonhydrostatic Anelastic Model under Segmentally-Constant Approximation: II. Dry version with adaptive activation and deactivation of segments, *submitted to Mon. Wea. Rev*.

Yano, J.-I., Bunoit, D. and Grabowski, W.W. 2008c, NAM-SCA: Nonhydrostatic Anelastic Model under Segmentally-Constant Approximation: III. Mosit version with Bulk microphysics, *in preparation*.

Yu, L. and Weller, R.A. 2007. Objectively Analyzed Air-sea Fluxes for the Global Ice-Oceans (1981-2005). *Bull. Amer. Meteor. Soc.,* 88, 527-539.

Zhang, G.J. and Mcphaden, M.J. 1995. The Relationship between Sea Surface Temperature and Latent Heat Flux in the Equatorial Pacific. *J. Climate*, **8**, 589–605.

Zhang, Y-C., Rossow, W.B., Lacis, A.A., Oinas, V. and Mishchenko, M.I. 2004. Calculation of radiative fluxes from the surface to top of atmosphere based on ISCCP and other global data sets: Refinements of the radiative transfer model and the input data. J. Geophys. Res., 109, D19105, doi:10.1029/2003JD004457,

Zhu, H. and Hendon, H. 2010: CAWCR Technical Report No. 022.

Zhu, H. and Sobel, A.H. 2011. Comparison of a single-column model in weak temperature gradient mode to its parent AGCM. *Q. J. R. Meteorol. Soc.* DOI:10.1002/qj.967

Zhu, H., Hendon, H. and Jacob, C. 2009: Convection in a parameterized and super-parameterized model and its role in the representation of the MJO. *J. Atmos. Sci*., **66,** 2796-2811.

Zilitinkevich, S.S., Elperin, T., Kleeorin, N. and Rogachevskii, I. 2007: Energy- and flux-budget (EFB) turbulence closure model for stably stratified flows. Part I: steady-state, homogeneous regimes. *Boundary-Layer Meteorol.*, **125**, 167-191.

The Centre for Australian Weather and Climate Research is a partnership between CSIRO and the Bureau of Meteorology.